2019-07-10

The Role of Lymph Node Subcapsular Sinus Macrophages in Limiting Tumor Progression through a B-cell Response

Louie, Dante Alexander Patrick

UNIVERSITY OF CALGARY

The Role of Lymph Node Subcapsular Sinus Macrophages in Limiting Tumor Progression through a B-cell Response

by

Dante Alexander Patrick Louie

A THESIS

SUBMITTED TO THE FACULTY OF GRADUATE STUDIES

IN PARTIAL FULFILMENT OF THE REQUIREMENTS FOR THE

DEGREE OF MASTER OF SCIENCE

GRADUATE PROGRAM IN MICROBIOLOGY AND INFECTIOUS DISEASES

CALGARY, ALBERTA

JULY, 2019

Abstract

Cancer immunotherapy targeting antitumor T-cells is demonstrated to be promising in treating several types of cancers. Adoptive T-cell transfer and immune checkpoint inhibitors are among the most successful immunotherapies today. However, these therapies are not effective in all patients and they can lead to devastating side effects in patients, including autoimmune diseases such as colitis. A better understanding of different aspects of cancer immunity can reveal additional targets for optimal cancer immunotherapy. One of these aspects is the tumor-draining lymph node - the first lymphoid organ that encounters tumor-derived antigens and generates the first wave of anti-tumor immunity. Recent publications have revealed that the activation of B-cells suppresses tumor growth in melanoma mice models. In my studies, using a C57BL/6 syngeneic E0771 breast cancer cell line, tumor-derived antigens were detected in the germinal center with $CD169^{+}$ subcapsular sinus macrophage in the tumor-draining lymph node. The importance of B-cells was demonstrated by using B-cell deficient mice, which significantly suppressed tumor growth compared to wild-type mice. Transferring wild-type B-cells to B-cell deficient mice recovered tumor growth. To determine if subcapsular sinus macrophages regulate B-cell activity, I depleted the lymph node subcapsular sinus macrophages with clodronate liposomes. Tumor growth and germinal center formation were increased when in the macrophage-depleted tumor-draining lymph nodes, suggesting subcapsular sinus macrophages limit B-cell activation in the lymph node. Collectively, my results reveal subcapsular sinus macrophages limit B-cell activity to prevent tumor growth, which can be a potential target for future cancer immunotherapy development.

Acknowledgements

I would like to thank everyone who contributed to the project discussed in this thesis. First, I thank my supervisors, Dr. Shan Liao and Dr. Pierre-Yves von der Weid for their guidance, support, and constructive criticism throughout my project. It is thanks to them that I was able to have a rewarding and successful graduate school experience. Additionally, I thank my committee members, Dr. Bryan Yipp and Dr. Douglas Mahoney, for their interest in my work and their advice in my committee meetings. I would also like to thank my internal examiner Dr. Morley Hollenberg for participating in the evaluation of my thesis.

I am appreciative of the funding sources that aided me in completing my studies: Graduate Student Scholarship and the Queen Elizabeth II Graduate Scholarship.

I would like to thank the past and present members of both the Liao group and the von der Weid group. I appreciated your questions, suggestions, and patience for all the lengthy practice sessions I had in preparation for committee meetings and seminars.

Finally, I would like to acknowledge my friends and family who have had nothing but support and confidence in me throughout my degree. Most importantly, I would like to thank April Tse, my loving girlfriend who supported me in every way during this project. I never could have survived without your constant encouragement.

Table of Contents

List of Tables

List of Figures and Illustrations

List of Symbols, Abbreviations, Nomenclature

ANOVA: Analysis of Variance
APC: Allophycocyanin
C57BL/6: Strain of mice acquired from Jackson Laboratory
CCL21: Chemokine (C-C motif) ligand 21
CCR7: C-C chemokine receptor 7
CD: Cluster of differentiation
CLL: Clodronate Liposomes
Cy3: Cyanine 3
Cy5: Cyanine 5
Cy7: Cyanine 7
DAPI: 4′,6-diamidino-2-phenylindole
DMEM: Dulbecco's Modified Eagle Medium
DT: Diphtheria toxin
DTR: Diphtheria toxin receptor
E0771: Spontaneous C56BL/6 syngeneic medullary breast adenocarcinoma cell line
ELISA: Enzyme Linked Immunosorbent Assay
FACS: Fluorescence-activated cell sorting
FBS: Fetal bovine serum
FITC: Fluorescein isothiocyanate
FSC: Forward scatter
GFP: Green Fluorescent Protein
Hm: Hamster
i.d.: Intradermal
i.p.: Intraperitoneal
i.v.: Intravenous
LN: Lymph node
Mac-1: Macrophage-1 antigen
μMT: Transgenic mice that lack the μ heavy chain and mature B-cells
ndLN: Non-draining lymph node
PBS: Phosphate buffered saline
PBS-L: Phosphate buffered saline Liposomes
PE: Phycoerythrin
PerCP: Peridinin Chlorophyll Protein Complex
Rt: Rat
Rb: Rabbit
SCS: Subcapsular sinus
SEM: Standard Error Mean
SSC: Side scatter
TuLN: Tumor-draining lymph node
WT: C57BL/6 strain wild-type mice

CHAPTER ONE: INTRODUCTION

1.1 Overview of Lymphatic Metastasis

Cancer metastasis is responsible for most cancer-related deaths in patients around the world, and is defined as the "spread of cancer cells from the primary tumor to surrounding tissues and distant organs". [1]. In fact, the accumulation of metastatic tumor cells in the sentinel lymph node is part of the TNM cancer staging system: T stands for tumor, N stands for lymph node, and M stands for metastasis. Each parameter is assigned a value resulting in a "stage" that can be used to describe the severity of the cancer. According to the staging system, a higher number of lymph node metastases is associated with a negative prognosis in cancer patients. The presence of lymph node metastases is correlated to advanced cancer progression stage and patient mortality. For instance, a study with 332 breast cancer patients determined a 23% 5-year-survival rate with lymph node metastases [2]. Despite the importance of using lymph node metastatic cells as a prognostic tool for cancer patients, the immunological function of tumor-draining lymph nodes remains unclear [3].

Metastatic tumor cells spread to the tumor-draining lymph node through lymphatic vessels. The lymphatic system is composed of the lymphatic vessels that direct pathogens and immune cells trafficking throughout the body, and the lymph nodes that house the immune cells. Studies on both components have been conducted to determine the mechanism of cancer lymphatic metastasis. Several clinical studies have demonstrated a correlation between VEGF-C expression and increased tumor progression in multiple tumor types [4-7]. Overexpressing VEGF-C increased the number of lymphatic vessels and the area of lymphatic vessels relative to tumor area, resulting in increased lymph node and lung metastases [8]. Moreover, human cervical tissue has demonstrated that tumor-associated macrophages, as defined by human cell markers such as

CD68, HLA-DR, CD16, CD23, CD45, can generate lymphangiogenesis factors, such as VEGF-C, to aid in the spread of cancer cells [4]. Once in the lymphatic vessels, evidence shows cancer cells may use chemokines for their movement, similar to the trafficking mechanism used by immune cells. For example, immune cell migration from the periphery to draining lymph nodes uses a CCR7/CCL21 receptor/ligand signaling in the lymphatic vessels to migrate. Homing of T- and B-cells was impaired in CCR7 deficient mice [9, 10]. CCR7 was also found to be expressed by axillary lymph node metastases in human breast cancer and more frequently co-stained with the cancer biomarker human epidermal growth factor receptor 2 (HER2/neu), suggesting increased CCR7 expression is correlated with enhanced cancer cell dissemination into the lymphatic system [11]. Cumulatively, clinical studies and animal models have revealed the capability of tumors to promote their own spread through lymphatic vessels [4-8, 11].

1.2 Immune Activation against Lymph-borne Pathogens

1.2.1 Antigen Trafficking to the Lymph Node

The lymphatic system is part of the circulatory system that runs parallel to the cardiovascular system in the body. Unlike the cardiovascular system, which utilizes arteries and veins to circulate blood, the lymphatic system consists of a network of unidirectional lymphatic vessels that traffics interstitial fluid, invading cells, and immune cells from peripheral tissue to the draining lymph nodes [12-14].

As mentioned earlier, a major contributor to lymph node homing is the CCR7 expression on immune cells and CCL21/CCL19 expression on lymphatic endothelial cells [9, 15-17]. Using CCR7 knockout models and immune stimulation, various types of immune cells, including neutrophils, dendritic cells, and T-cells have been shown to express the CC chemokine receptor to traffic in the lymphatic vessels along a CCL21 concentration gradient [9, 10, 18].

Alternatively, macrophages migrate to the lymph nodes using an integrin adhesion molecule called Mac-1, demonstrated by the presence of transferred GFP^+ macrophages recovered in the lymph node post-LPS challenge [19]. After capturing pathogens, these immune cells traffic to the lymph nodes to initiate an immune response. However, not all pathogens are captured by immune cells in the tissue. Free-floating antigens in tissue can enter lymphatic vessels with fluid flow and traffic to the lymph node without the assistance of a proper antigen-presenting cell.

In the lymph node, lymph from the afferent lymphatic vessels fills the subcapsular sinus. Lining the floor of subcapsular sinus are a subset of macrophages, appropriately denoted as the subcapsular sinus macrophages. These macrophages sample oncoming lymph for free-floating antigens [20, 21]. Once they encounter lymph-borne antigens, these macrophages exhibit a variety of functions, depending on the type of challenge.

1.2.2 Characterization and Development of Lymph Node Subcapsular Sinus Macrophages

There are several immune cell types that line the lymph node sinus, including two distinct populations of macrophages that can be distinguished via different cell surface markers. Subcapsular sinus macrophages express Mac1 (CD11b/CD18), Siglec-1 (CD169), but lack the typical murine macrophages marker, F4/80 [22]. Some of these cells are $CD11c^+$, indicating a possibility of a dendritic cell phenotype [23, 24]. Yet, these cells are still defined as macrophages due to the dependence on the "macrophage colony-stimulating factor", a cytokine also known as CSF-1 [22, 25, 26]. On the other hand, medullary sinus macrophages mainly express F4/80 and Mac1, better indicating their macrophage phenotype. Some of them still express CD169 at a low level, hence distinguishing medullary sinus macrophages as $CD169^{low/-}F4/80^+$, while subcapsular sinus macrophages are defined as $CD169^+F4/80^-$ [20].

In addition to phenotype, sinus macrophages differ functionally. Macrophages are generally classified into two types: classically activated M1 macrophages, which produce pro-inflammatory cytokines and contribute to pathogen resistance, and alternatively activated M2 macrophages, which typically show low phagocytic activity, have limited pro-inflammatory cytokine production, promote tissue regeneration, and produce anti-inflammatory cytokines [27]. Different from the general classification, lymph node medullary sinus macrophages show high lysozyme content and the ability to process antigens, but do not demonstrate the ability to produce pro-inflammatory cytokines [28, 29]. Conversely, subcapsular sinus macrophages show limited phagocytic activity, but definitely produce pro-inflammatory cytokines, namely type I interferons [22, 30, 31]. Therefore, both types of sinus macrophages exhibit partial M1 macrophage functions, yet neither perfectly fit the current dogma.

Several cytokines and their receptors are demonstrated to regulate the development of subcapsular sinus macrophages. Demonstrated in transgenic mice with a recessive osteopetrotic mutation (*op/op*), CSF-1 deficient mice show a significant reduction in subcapsular sinus macrophages. Blocking the CSF-1 ligand from binding to the CSF-1 receptor also significantly depleted the subcapsular sinus macrophages, while the medullary sinus macrophages remained intact [25]. Blocking the signaling with a soluble anti-CSF1R antibody only depleted the subcapsular sinus macrophages, further indicating different developmental signaling pathways [26]. Along with CSF-1, subcapsular sinus macrophages also require lymphotoxin-β-receptor signaling for development. Chimeric mice lacking lymphotoxin receptor LTβR (*ltbr*$^{-/-}$) show a deficiency in the subcapsular sinus macrophages, but not medullary sinus macrophages, despite both expressing LTβR [22]. The ligand for LTβR, $LT\alpha_1\beta_2$, are present on lymph node B-cells that underly the lymph node subcapsular sinus. B-cell deficient μMT mice show significantly

fewer $CD169^{+}F4/80^{-}$ subcapsular sinus macrophages [31]. Ablating lymphotoxin signaling in wild-type mice with LTβR-Ig to block downstream signaling showed a similar subcapsular sinus macrophage deficiency, but the medullary sinus macrophage population seems unaffected [31]. Overall, CSF-1/CSF-1 receptor and $LT\alpha_1\beta_2$/LTβR are necessary signaling pathways for subcapsular sinus macrophages development and maintenance.

1.2.3 Lymph Node Subcapsular Sinus Macrophages Limit Microbial Systemic Spread

Subcapsular sinus macrophages have been widely studied in antimicrobial immunity, mainly in anti-viral and anti-bacterial responses. Initially, the function of subcapsular sinus macrophages was discovered in the context of limiting virus spread from the lymph node to the blood circulation or other organs post-subcutaneous infection. Through multiphoton intravital microscopy, $CD11b^{+}CD169^{+}MHCII^{+}$ cells were identified on the floor of the popliteal lymph node subcapsular sinus and their function in stopping live vesicular stomatitis virus (VSV) was recorded [32]. Depleting these macrophages reduced the amount of viral titers recovered in the draining lymph node, which were instead found in the brain and spinal cord [30]. Similar observations have been made in other viral infections such as adenovirus, vaccinia virus, and murine cytomegalovirus (MCMV), as evidence indicates each type of virus is limited to the lymph node before spreading systemically [32, 33].

The ability to prevent the systemic spread of microbes is not limited to viruses as similar observations have been made with bacteria. *Pseudomonas aeruginosa* was limited to the lymph node subcapsular sinus when the macrophage layer was intact, but were found in the lymph node parenchyma and blood 8 hours post-injection when the macrophages were depleted with clodronate liposomes [34]. Bacterium components such as lipopolysaccharides are also localized with the subcapsular sinus macrophages [35]. Studies on barrier function of the subcapsular sinus

macrophages also reveal a potential function for the phenotype-defining CD169 cell marker as CD169 interacts with α2,3-linked sialic acids expressed on cell surfaces or microbes. Biotinylated exosomes were bound to subcapsular sinus macrophages, but biotinylated bovine serum albumin was not, suggesting $CD169^+$ macrophages captured extracellular vesicles and microbes rather than free flow proteins [36]. As CD169 is an adhesion molecule, this provides a potential mechanism for the capture and retention of lymph-borne pathogens at the subcapsular sinus. Cumulatively, subcapsular sinus macrophages play important roles in limiting the spread of lymph-borne microbes.

1.2.4 Lymph Node Subcapsular Sinus Macrophages and Lymphatic Metastasis

As subcapsular sinus macrophages have been shown to limit the spread of microbes via the lymphatic system, it is possible that this function extends to metastasizing tumor cells. Several clinical studies observe a correlation between cancer patients' sentinel lymph node $CD169^+$ macrophages and fewer lymph node metastases. Colorectal carcinoma patient tumor-draining lymph nodes were stained to quantify the expression of $CD169^+$ cells to find a correlation with clinicopathological features. In patients with low $CD169^+$ cells, there was a significant correlation with tumor growth and lymph node metastasis [37]. This observation was not limited to colorectal carcinoma; another study on 167 breast ductal carcinoma patients found similar results. A higher density of $CD169^+$ macrophages in the tumor-draining axillary lymph nodes was correlated with smaller tumor size, no lymph node metastasis and an early TNM clinical stage [38]. Therefore, clinical studies have shown the importance of $CD169^+$ cells in limiting lymphatic metastasis. The mechanism of their action, however, remains unclear.

1.3 Antitumor Immunity and Immunotherapies

1.3.1 Lymph Node Subcapsular Sinus Macrophages Activate Antitumor Immunity

Recently, animal models have been used to show the role of subcapsular sinus macrophages in activating antitumor immunity. More specifically, X-ray irradiated ovalbumin (OVA)-transfected EG7 T-cell thymoma cells were captured by $CD169^+$ macrophages and induced $CD8^+$ T-cell proliferation. Vaccinating mice with these dead tumor cells 10 days prior to live EG7 cell implantation allowed wild-type mice to reject the tumor. When subcapsular sinus macrophages were depleted in a CD169-DTR mouse model, where diphtheria toxin injection selectively depletes CD169-expressing cells, vaccination with irradiated EG7 tumor cells was not able to reduce tumor growth.

Analysis on the $CD169^+$ macrophages and T-cells further revealed their interaction in antitumor immunity. Given that these tumor cells were conjugated with ovalbumin, OTI T-cells ($CD8^+$ T-cells specific to OVA) were transferred into wild-type and CD169-DTR mice. Irradiated OVA-EG7 cells did not cause OTI T cell proliferation in DT-treated CD169-DTR mice compared to wild-type, therefore revealing the role of subcapsular sinus macrophages in activating an antitumor T-cell response [23].

1.3.2 Antitumor T-cell Immunity

Currently, the predominate studies on antitumor immunity focus on the involvement of T-cells. Clinical studies with 147 metastatic melanoma patients revealed the highest proportion of tumor-infiltrating cells as T-cells in both the primary tumor and the metastatic sites. There was a positive correlation with higher intratumoral $CD8^+$ T-cells and patient survival [39]. Earlier studies done on 109 non-small-cell lung carcinoma patient samples show similar results. The number of tumor-infiltrating $CD8^+$ and $CD4^+$ T-cells were counted in five field-of-views at 200x

magnification for each patient, and using the median as the standard, the samples were divided into high and low T-cell groups. Fewer lymph node metastases and lower TNM stage was significantly correlated with higher intratumoral $CD8^+$ T-cell number [40]. These studies demonstrate the importance of T-cells in antitumor immunity.

On the other hand, $CD4^+$ T-cells appear to have a role in producing cytokines necessary for surviving tumors. $CD4^+$ T-cells are required to promote the effect of tumor vaccination, since CD4 knockout mice failed to improve survival rate post-tumor vaccination compared to wild-type or CD8 knockout mice. Quantitative PCR analysis on the CD8 knockout mice and wild-type mice show comparable levels of IFN-γ and IL-4 mRNA post-vaccination, but the IFN-γ and IL-4 mRNA level was substantially reduced in CD4 knockout mice, suggesting $CD4^+$ T-cells are responsible for producing these cytokines. Knocking out either cytokine resulted in a similar decrease in survival rate [41].

Overall, both mouse models and human cancer patients demonstrate the importance of T-cells in antitumor immunity.

1.3.3 Cancer Immunotherapies targeting T-cells

There are several popular methods that utilize $CD8^+$ T-cells for cancer immunotherapy: namely, adoptive T-cell therapy and immune checkpoint inhibitors. The method of adoptive T-cell therapy is based on the introduction of primed antitumor T-cells for a tumor-targeted attack. For example, a study implanted OVA protein (OVA)-expressing EG7 T-cell lymphoma into a mouse. The *in vivo* effect of naïve, memory, and tumor-infiltrating $CD8^+$ cells were assessed by adoptively transferring these cell types from an OTI T-lymphocyte specific (Thy1.1) mouse into the tumor-bearing mouse. Naïve T-cells delayed tumor growth for at least 35 days compared to

memory and tumor-infiltrating $CD8^+$ T-cells [42]. These results suggest $CD8^+$ T-cells limit tumor growth, albeit one subset is preferable compared to others.

Studies have also shown that the source of these antitumor T-cells could be the tumor-draining lymph node. A group genetically modified murine B16 melanoma cells with a bacterial superantigen, staphylococcal enterotoxin A (SEA), to assess lymph node antitumor activity in response to immunogenic tumor cells. Irradiated B16 cells and SEA-B16 cells were subcutaneously injected and the tumor-draining lymph node was collected after 10 days. Lymph node T-cells were purified, then stimulated with anti-CD3, anti-CD28, and IL-2. T-cell proliferation was higher in SEA-B16 tumor-draining lymph nodes in response to all three stimuli. Hence, it appears tumor immunogenicity greatly influences the production of antitumor T-cells. Adoptively transferring either of these stimulated T-cells into tumor-bearing mice induced significant tumor regression, however the effects of SEA-B16 lymph node T-cells were much more prominent [43]. Cumulatively, these results show the importance of lymph node T-cells and immunogenicity in antitumor immunity.

As an extension of adoptive T-cell therapy, chimeric antigen receptor T-cell therapy also uses a reinfusion of T-cells into the patient. However, there are is a key difference; T-cells are genetically modified to express a chimeric antigen receptor specific to a tumor antigen to increase specificity. The development of this technique marked a new era of cancer immunotherapy. In clinical studies, a patient with chronic lymphocytic leukemia were infused with chimeric antigen receptor T-cells specific to CD19, a common B-cell antigen. Twenty-three days after cell infusion, the patient showed no chronic lymphocytic leukemia in the bone marrow [44]. These success stories motivated further development of this technique. Several clinical studies are being conducted on chimeric antigen T-cell therapies for other tumor types. Multiple

tumor-associated antigens for neuroblastoma are being tested to determine the best target for therapy [45]. Strategies like chimeric antigen T-cell therapy only further exemplify the efficiency and potency of antitumor T-cells.

In addition to increasing the number of circulating cytotoxic T-cells via adoptive T-cell transfer, another immunotherapy works on improving the efficacy of the host antitumor T-cells. In the previously discussed study on OVA-expressing EG7 T-cell lymphoma, human naïve, memory, and tumor-infiltrating $CD8^+$ T-cells were cultured and observed for the presence of inhibitory receptors. Naïve $CD8^+$ T-cells presented significantly fewer programmed death (PD-1) and cytotoxic T-lymphocyte-associated protein 4 (CTLA-4) receptors compared to memory and tumor-infiltrating $CD8^+$ T-cells [42]. The purpose of these receptors is to, when bound, suppress immune responses. These receptors are known as immune checkpoints and blocking them with inhibitors can improve antitumor immunity, thus resulting in a widely studied cancer immunotherapy. T-cell CTLA-4 is expressed on active T-cells and binds to CD80/B7-1 or CD86/B7-2 on antigen presenting cells. If this inhibitory signaling overcomes the costimulatory signal between B7 and CD28, T-cell exhaustion occurs. Similarly, PD1 is found on T-cells, and upon encountering its ligand (PD-L1) on tumor cells, inhibits T-cell proliferation and activation. Using immune checkpoint inhibitors prevents T-cell immunosuppression in the tumor, consequently acting as an antitumor immunotherapy [46]. The research on this immunotherapy has developed enough to the point of clinical trials. Metastatic melanoma patients were treated with Ipilimumab, an anti-CTLA-4 drug. Patients were randomly administered 3mg/kg ipilimumab with a melanoma antigen glycoprotein 100 (gp100) vaccine, ipilimumab with a gp100 placebo, or ipilimumab placebo with gp100 every 3 weeks for 12 weeks. With ipilimumab, the median overall survival was approximately 10 months. The survival rate was

significantly lower in patients with gp100 alone, at approximately 6.4 months [47]. Additionally, anti-PD-1 antibody BMS-936558 has also been introduced to clinical trials. Various types of cancer patients, such as melanoma, non-small-cell lung cancer, renal-cell cancer, prostate cancer, and colorectal cancer, were treated with the anti-PD-1 antibody. One in four patients treated showed a decrease in tumor lesions lasting for one year or more. Between 18 to 28% of patients responded to the therapy, but approximately 14% of the patients experienced drug-related adverse effects. Unfortunately, this leaves three out of four patients unresponsive to the anti-PD-1 treatment, while others may suffer from severe side-effects [48].

In general, blocking the natural immune suppression in immune checkpoint blockade can result in adverse effects on the immune system, and potentially cause an autoimmune side-effect. For example, some clinical studies have shown that in the patients treated with ipilimumab, immune-related adverse effects occurred, likely a consequence of abrogating T-cell exhaustion. Diseases such as colitis, vitiligo, and endocrine immune-related effects were present – all representative of an overactive immune system [47]. Similarly, PD-1 also induces a couple of drug-related adverse effects like colitis and vitiligo [48]. These problems are not limited to immune checkpoint inhibitors. Chimeric antigen receptor T-cell therapy also induces adverse side-effects. As many cancer cells share similar antigens with host cells, it is difficult to specifically target cancer cells. A patient with chronic lymphocytic leukemia was treated with chimeric antigen receptor T-cell therapy, and their B-cells targeted via the CD19 antigen. Up to 6 months after treatment, the patient's B-cells remained depleted. This treatment, while removing the problematic cancer cells, also open up the possibility for severe secondary infections [44]. In summary, despite overwhelming success in several clinical trials, T-cell cancer immunotherapies are not perfect. A large population of patients do not respond to immune checkpoint inhibitor

treatment, and those who do may also incur immune-related diseases. This emphasizes the importance of improving all facets of antitumor immunity as it can reveal new targets for cancer immunotherapies that may be more suitable for certain cancer patients.

1.3.4 Antitumor B-cell Immunity

Understanding why most patients do not respond to immunotherapies targeting T-cells requires a better understanding of cancer immunity in general. Compared to T-cell immunity in cancer progression, the role of B-cells in tumor immunity is underdeveloped. In fact, most of the studies on B-cell activity in tumor progression using mouse models observe an inhibition of antitumor immunity. For example, mice with methylcolanthrene-induced murine fibrosarcoma (MCC) were treated with anti-CD20 monoclonal antibodies to deplete B-cells 3 days prior to tumor implantation. Tumor growth in B cell depleted mice were accelerated compared to control mice. In contrast, depleting B-cells 9 days post-tumor implantation reduced tumor growth, suggesting B-cell activation during tumor growth has a pro-tumor effect. Based on this observation, the tumor-draining lymph nodes were studied in both B-cell depletion scenarios. Depleting B-cells with anti-CD20 before tumor inoculation increased the number of activated $CD8^+$ and $CD4^+$ T-cells, while simultaneously increasing the number of $CD25^+$ regulatory T-cells. Meanwhile, depleting B-cells after tumor implantation increased the number of IFNγ-expressing $CD8^+$ T-cells and decreased regulatory T-cells. Not only were the number of $CD8^+$ T-cells increased, their activity also demonstrated an increase in cytotoxicity against MCC tumor cells compared to the control group [49]. Based on these results, it appears that B-cells produced post-tumor implantation interfere with lymph node $CD8^+$ T-cell production and promote regulatory T-cells, thus leading to a pro-tumor effect.

As a potential explanation for this pro-tumor effect, a recent study noted an accumulation of tumor-derived vesicles in the tumor-draining lymph node cortex upon subcapsular sinus macrophage depletion. Fluorescently labeling a vesicular membrane-associated protein, CD63, with green fluorescent protein (GFP) on a B16F10 melanoma tumor cell line, the authors were able to track the movement of tumor-derived vesicles. Whole mount multiphoton imaging showed a restriction of tumor-derived vesicles at the subcapsular sinus, which was previously shown to be captured by the subcapsular sinus macrophages [36, 50]. This was further supported by macrophage-depletion experiments. Subcapsular sinus macrophages were depleted with clodronate liposomes, or with diphtheria toxin in CD169-DTR mice. End tumor volume was significantly higher, which is consistent with previous studies that subcapsular sinus macrophages limit tumor growth [23]. Additionally, the fluorescently labeled tumor-derived vesicles could be found up to 160μm deep into the clodronate liposome-treated tumor-draining lymph node cortex. PBS liposome-treated tumor-draining lymph nodes restrict the tumor-derived vesicles at the subcapsular sinus with the presence of the subcapsular sinus macrophages. As B-cell follicles lie just underneath the lymph node subcapsular sinus, the authors hypothesized the activation of B-cells in response to the tumor-derived vesicles. Blood plasma cells and plasma IgG levels were increased in macrophage-depleted mice, implying a B-cell activation. When transferring purified IgG from tumor-bearing subcapsular sinus macrophage-depleted mice to B16F10 tumor-bearing wild-type mice, the end tumor volume was significantly larger [50]. Collectively, this evidence furthers the idea of pro-tumor B-cells, and the role of subcapsular sinus macrophages in limiting tumor B-cell activation.

From the studies summarized above, it is clear there is a correlation between B-cells and a pro-tumor phenotype. Lymph node subcapsular sinus macrophages appear to limit the

activation of B-cells. Can B cells promote breast cancer growth? How do subcapsular sinus macrophages limit B-cell activation ? Answering these questions can unravel the complexities of tumor B-cell activation and can provide alternative targets for future cancer immunotherapy development.

1.4 Hypothesis and aims

1.4.1 Hypothesis

Lymph node subcapsular sinus macrophages limit E0771 breast cancer growth by limiting B-cell activation.

1.4.2 Aims

Aim 1: To determine B-cell activation in the E0771 tumor-draining lymph node.

Aim 2: To determine the role of B-cells in E0771 breast cancer growth.

Aim 3: To determine the role of subcapsular sinus macrophages in B-cell activation and E0771 breast cancer growth.

CHAPTER TWO: METHODS AND MATERIALS

2.1 Statement of Compliance and Ethical Use of Animals

C57BL/6J mice (purchased from The Jackson Laboratory) and μMT mice (a gift from Dr. Bryan Yipp) were bred at the Health Science Animal Resource Center at the University of Calgary. All experiments were performed using 6- to 8-week-old female mice. All animal protocols were reviewed and approved by the University of Calgary Animal Care and Ethics Committee and conformed to the guidelines established by the Canadian Council on Animal Care.

2.2 General List of Solutions and Chemical Reagents

All materials purchased throughout this project are listed below with their catalog number and supplier. All materials were reconstituted and stored according to their technical data sheets and published protocol.

Table 1: General List of Materials Used

Cell Culture		
Item	**Catalog Number**	**Supplier**
E0771 Murine Breast Cancer Cell Line	940001	CH3 BioSystems
Dulbecco's Phosphate Buffered Saline	D8662-500ML	SIGMA Life Science
Dulbecco's Modified Eagle's Medium – high glucose	D5796-500ML	SIGMA Life Science
10x Trypsin – EDTA Solution	T4174-100ML	SIGMA Life Science
Bovine Serum Albumin	F1051-500ML	SIGMA Life Science
Dimethyl sulfoxide (DMSO)	D2650-5x10ML	SIGMA Life Science
Lipofectamine 2000 Reagent	11668027	ThermoFisher Scientific
500mL Rapid-Flow Filter Unit 0.2μm aPES membrane, 75mm dia	566-0020	ThermoFisher Scientific

75cm^2 Cell Culture Flask, Straight Neck, Tissue Culture Treated	3276	Corning Life Sciences
VWR Cell scraper	10062-906	VWR
15mL Falcon Polypropylene Conical Tube	352097	Corning Life Sciences
50mL Falcon Polypropylene Conical Tube	352098	Corning Life Sciences
VWR 2mL Aspirating Pipet	414004265	VWR
ACK Lysing Buffer	A10492-01	gibco
Animal Work		
Item	**Catalog Number**	**Supplier**
C57BL/6J mice	000664	The Jackson Laboratory
BD 1ml Slip Tip Sterile Syringes	309659	BD
BD 30G x 1/2 in regular bevel needles	305106	BD
BD Lo-Dose U-100 Insulin Syringe	329461	BD
Hair Removal Cream		Veet
Kimwipes Delicate Task Wipers	34155	Kimberly-Clark Professional
Heparin LEO	00453811	LEO Pharma Inc.
Control and Clodronate Liposomes	CP-005-005	Liposoma Research
Immunofluorescent Staining		
Item	**Catalog Number**	**Supplier**
Purified anti-mouse CD8a	100702	BioLegend
Purified anti-mouse CD169 (Siglec-1)	142402	BioLegend
Anti-Collagen I antibody	ab34710	Abcam
Purified anti-mouse/human GL7 Antigen (T and B cell Activation Marker)	144602	BioLegend
Lectin from *Arachis hypogaea* (peanut) (PNA)	L6135-1MG	SIGMA Life Science
Purified Rat Anti-Mouse CD45R	550286	BD Pharmingen
Rabbit Anti-Mouse Lymphatic Vessel Endothelial Hyaluronan Receptor 1 Affinity Purified pAb	PA0846	Cell Sciences

Alexa Fluor 488-conjugated AffiniPure Goat Anti-Rat IgG (H+L)	112-545-003	Jackson ImmunoResearch
Alexa Fluor 488-conjugated AffiniPure Donkey Anti-Rabbit IgG (H+L)	711-545-152	Jackson ImmunoResearch
Cy3-conjugated AffiniPure Goat Anti-Rat IgG (H+L)	112-165-003	Jackson ImmunoResearch
Cy3-conjugated AffiniPure Donkey Anti-Rabbit IgG (H+L)	711-165-152	Jackson ImmunoResearch
Cy5-conjugated AffiniPure Donkey Anti-Rat IgG (H+L)	712-175-153	Jackson ImmunoResearch
Cy5-conjugated AffiniPure Donkey Anti-Rabbit IgG (H+L)	711-175-152	Jackson ImmunoResearch
PE Streptavidin	554061	BD Pharmingen
Normal Mouse Serum	015-000-120	Jackson ImmunoResearch
Tissue-Tek O.C.T. Compound	4583	Sakura Finetek USA, Inc.
Microscope Slides	12-550-15	Fisher Scientific
Edge-Rite Disposable Microtome Blades	4275H	ThermoScientific
Vectashield with DAPI	VECTH1200	BioLynx

Flow Cytometry

Fluorophore	**Marker**	**Clone**	**Catalog Number**	**Supplier**
FITC	CD169	3D6.112	142406	BioLegend
	CD11c	HL3	553801	BD Biosciences
	CD8	53-6.7	553031	BD Biosciences
PE	F4/80	BM8	123110	BioLegend
	CD19	6D5	115508	BioLegend
	CD8	53-6.7	553033	BD Pharmingen
PerCP Cy5.5	CD169	3D6.112	142410	BioLegend
	CD4	RM4-5	553052	BD Pharmingen
	CD45	30-F11	557235	BD Pharmingen
PE Cy7	CD11c	N418	117318	BioLegend
	CD45	30-F11	103114	BioLegend
	CD25	PC61	102016	BioLegend
APC	F4/80	BM8	123116	BioLegend
	CD11c	N418	117310	BioLegend
	CD169	3D6.112	142418	BioLegend
	CD19	6D5	115512	BioLegend
APC Cy7	CD11b	M1/70	557657	BD Pharmingen
	CD45	30-F11	557659	BD Pharmingen

Purified Rat Anti-Mouse CD16/CD32 (Mouse BD Fc Block), Clone: 2.4G2	553142	BD Pharmingen
Magnetic-Activated Cell Sorting (MACS)		
Item	**Catalog Number**	**Supplier**
CD45R (B220) MicroBeads, mouse	130-097-152	Miltenyi Biotec
LS Columns	130-042-401	Miltenyi Biotec
CFSE	ab113853	Abcam
Enzyme-linked Immunosorbent Assay (ELISA)		
Mouse IgG ELISA Kit	501240	Cayman Chemical
Software		
Software	**Version**	**Supplier**
GraphPad Prism	6.01	GraphPad Software
ImageJ	1.51n	ImageJ
FlowJo	10.2	FlowJo
Benchwork		
Item	**Catalog Number**	**Supplier**
VWR 5mL Serological Pipet	89130-896	VWR
VWR 10mL Serological Pipet	89130-898	VWR
VWR Microcentrifuge Tubes	87003-296	VWR
0.1-10µL VWR Tips	53509-070	VWR
1-200µL VWR Tips	53503-790	VWR
100-1000µL VWR Tips	83007-382	VWR
Nitrile Examination Gloves	82026-426	VWR

2.3 Mouse Anesthesia and Euthanasia

Anesthetic solution was made by mixing 1mL ketamine (100mg/mL), 50µL xylazine (100mg/mL), and 9mL 0.9% NaCl saline. One hundred and fifty microliters (150 µL) of solution was intraperitoneally injected to anesthetize the animals.

To euthanize, animals were anesthetized using the same method, followed by cervical dislocation.

2.4 Tumor Cell Culture

E0771 is a C57BL/6J syngeneic, triple negative, spontaneously developing medullary breast adenocarcinoma. Triple negative breast cancer lack estrogen receptors, progesterone

receptors and HER2 amplifications; common targets for cancer therapy. The animals in this project are C57BL/6J mice, or μMT mice with a C57BL/6J background, hence the use of this cell line. E0771 has been previously described as a good model for studying metastatic breast cancer [51]. E0771 stocks were purchased from CH3 Biosystems (CH3 Biosystems 940001).

E0771 cells were cultured at 37^{o}C and 5% CO_2 in a T75 flask. High glucose (4500mg/L) Dulbecco's Modified Eagle's Medium was supplemented with 10% heat inactivated FBS, then filtered through a 0.22μm filter. Cells were harvested at 80-90% confluency for use, storage, or passaging. To store cells, cells were resuspended in 7.5% DMSO in FBS, transferred into a cryovial, and placed in a freezing box at -80^{o}C.

2.5 Tumor Implantation and Growth

6-8-week-old female mice were anaesthetized, and the fourth right mammary fat pad of the mouse was exposed by gently applying Nair hair removal cream to the area. Five minutes later, hair was rubbed off using a damp Kimwipe.

To prepare E0771 cells for implantation, media was aspirated, and cell monolayer was briefly washed with 5mL PBS. PBS was aspirated and 2mL 10X Trypsin was added. E0771 cells were incubated at 37^{o}C and 5% CO_2 for 5 minutes. Ten milliliters (10mL) of media is added to the flask to help detach cells from the flask surface and transfer the cells into a 15mL Falcon tube. Cells were centrifuged at 1500RPM at 4^{o}C for 5 minutes, and supernatant was aspirated. Pellet was resuspended in PBS to wash cells, and cells were centrifuged again at 1500RPM for 5 minutes. E0771 cells were then resuspended in PBS to a concentration of 1.0 x 10^6 cells per 50μL. One million (1.0 x 10^6) cells in 50μL PBS were then injected subcutaneously using an

insulin syringe into the exposed fourth right mammary fat pad. Animals were marked with ear punches to track tumor growth over 21 days.

Seven days post-tumor implantation, tumor length and width were measured using a caliper. Tumors were then measured every 2 days (i.e. day 9, 11, 13, 15, 17, 19, 21). To calculate tumor volume, tumor depth was assumed to be the average of measured tumor length and width, and ellipsoid volume was calculated. To simplify calculations, π was rounded down to 3.

Sample Calculation of Tumor Volume:

Length: 7.0mm

Width: 5.5mm

Depth: $\frac{7.0mm+5.5mm}{2} = \frac{12.5mm}{2} = 6.25mm$

Volume = $\frac{4}{3}\pi r_1 r_2 r_3 = 4\left(\frac{d_1}{2}\right)\left(\frac{d_2}{2}\right)\left(\frac{d_3}{2}\right) = 4\left(\frac{7.0mm}{2}\right)\left(\frac{5.5mm}{2}\right)\left(\frac{6.25mm}{2}\right) = 120.3125mm^3$

2.6 Clodronate Liposome Treatment

2.6.1 Local Clodronate Liposome Treatment

Seven days prior to tumor implantation, 6-8-week-old female C57BL/6J mice were anaesthetized using the ketamine/xylazine solution. The flanks of the mice were shaved using an electric shaver. Fifty microliters (50μL) of PBS liposome (control) or clodronate liposome (Liposoma Research CP-005-005) was intradermally injected into the right hind flank to deplete inguinal lymph node subcapsular sinus macrophages prior to tumor implantation.

Liposomes were injected into the right hind flank every 7 days afterwards to maintain macrophage depletion over 21 days of tumor growth.

2.6.2 Systemic Clodronate Liposome Treatment

Seven days prior to tumor implantation, 6-8-week-old female C57BL/6J mice were intraperitoneally injected with 150µL of PBS liposome (control) or clodronate liposomes (Liposoma Research CP-005-005).

Liposomes were intraperitoneally injected every 7 days afterward to maintain macrophage depletion over 21 days of tumor growth.

2.7 B-cell/Plasma Isolation and Adoptive Transfer

2.7.1 B-cell isolation

Spleens were harvested from C57BL/6J mice and pushed through a 40µm cell strainer into 5mL PBS. Cells were transferred into a 15mL Falcon tube and cell suspension was incubated with 5mL ACK lysing buffer (gibco A10492-01) for 5 minutes at room temperature. Cells were centrifuged at 300g for 10 minutes at 4^{o}C. Supernatant was aspirated and pellet was resuspended in MACS buffer (0.5% BSA, 2mM EDTA in PBS, pH 7.2) at 10^7 cells per 90µL.

Ten microliters (10µL) CD45R (B220) (Miltenyi Biotec 130-097-152) Microbeads per 10^7 cells was added to cell suspension and incubated at 4^{o}C for 15 minutes. Cells were then washed with 1mL MACS buffer per 10^7 cells and centrifuged at 300g for 10 minutes. Supernatant was aspirated and cells were resuspended in 500µL of MACS buffer.

LS column (Miltenyi Biotec 130-042-401) was placed in a magnetic field and rinsed with 3mL MACS buffer. Cell suspension was applied to the LS column and CD45R/B220^{-} flow-through was collected in a 15mL Falcon tube. Fifty microliters (50µL) of CD45R/B220^{-} flow-through was collected for testing. Then, column was washed 3 times with 3mL MACS buffer.

Column was removed from the magnetic field and placed on a collection tube for CD45R/B220^{+} cell collection. Five milliliters (5mL) MACS buffer was added to the column and plunger was used to flush out cells into collection tube. Fifty microliters (50µL) of elution was collected for testing. Flow-through and elution samples were stained with CD19 PE antibody and analyzed with flow cytometry to confirm B-cell isolation.

2.7.2 B-cell adoptive transfer

B220^{+} cells in collection tube were centrifuged at 300g for 10 minutes at 4^{o}C. Cells were resuspended at 1.5x10^{7} cells per 150µL PBS.

6-8-week-old µMT mice were anesthetized and 1.5x10^{7} B220^{+} cells were intravenously injected via tail vein injection. Tumors were introduced 2 weeks post-B-cell transfer to ensure B-cells had enough time to settle.

2.7.3 Mouse plasma isolation

Mice were anesthetized. Approximately 500µL of blood was collected via optical bleed into an Eppendorf tube with 50µL Heparin (LEO 00453811). Blood was centrifuged at 13000 RPM for 5 minutes at 4^{o}C.

Blood plasma supernatant was separated and collected into a separate Eppendorf tube and stored at -80^{o}C until use.

2.7.4 Mouse plasma transfer

Mice were anesthetized. One hundred and fifty to two hundred microliters (150-200µL) of plasma was transferred intravenously via a tail vein injection.

2.8 CFSE Labeling

Cells are resuspended in 4mL PBS. One microliter (1μL) CFSE is added and mixed with cells gently. Cells are incubated in the dark for 10 minutes at room temperature.

Ten milliliters (10mL) 10% FBS in DMEM is added to the cells. Mixture is incubated in the dark for 5 minutes at room temperature. Cells are centrifuged at 1500RPM for 5 minutes at 4^{o}C. Supernatant is aspirated. Cells are washed twice by resuspending in 10mL PBS and centrifuging at 1500RPM for 5 minutes at 4^{o}C. Cells are counted using a hematocytometer, then resuspended in appropriate volume of PBS for injection.

2.9 Cryosections and Immunofluorescent Staining

2.9.1 Cryosections

Harvested lymph nodes were fixed with 4% formalin in PBS for 1 hour or unfixed and immediately placed into PBS. Samples were put into a cryomold with O.C.T. and flash-frozen in 100% ethanol with dry ice. Ten micrometer (10μm) lymph node sections were cut with a cryostat at -20^{o}C.

Cryosections were then fixed in acetone at -20^{o}C for 20 minutes and left to air-dry. Slides were stored at -80^{o}C until use.

2.9.2 Immunofluorescent Staining

A well was drawn around the sample using a hydrophobic pen. Samples were blocked using 5% normal mouse serum in PBS for at least 1 hour in a humidifier. Primary antibodies (Purified anti-mouse CD8a [BioLegend 100702], Purified anti-mouse CD169 [BioLegend 142402], Anti-Collagen I antibody [Abcam ab34710], Purified anti-mouse/human GL7 Antigen

[BioLegend 144602], Lectin from *Arachis hypogaea* [SIGMA L6135-1MG], Purified Rat Anti-Mouse CD45R [BD Pharmingen 550286], Rabbit Anti-Mouse Lymphatic Vessel Endothelial Hyaluronan Receptor 1 Affinity Purified pAb [Cell Sciences PA0846]) were diluted 1:200 in 5% normal mouse serum in PBS and samples were incubated with primary antibodies overnight at 4^{o}C in a humidifier.

The next day, primary antibodies are washed off using 3x PBS washes for 10 minutes each. Secondary antibodies (Alexa Fluor 488-conjugated AffiniPure Goat Anti-Rat IgG [Jackson 112-545-003], Alexa Fluor 488-conjugated AffiniPure Donkey Anti-Rabbit IgG [Jackson 711-545-152], Cy3-conjugated AffiniPure Goat Anti-Rat IgG [Jackson 112-165-003], Cy3-conjugated AffiniPure Goat Anti-Rat IgG [Jackson 711-165-152], Cy5-conjugated AffiniPure Donkey Anti-Rat IgG [Jackson 712-175-153], Cy5-conjugated AffiniPure Donkey Anti-Rabbit IgG [Jackson 711-175-152], PE Streptavidin [BD Pharmingen 554061]) were diluted 1:400 in 5% mouse serum in PBS and incubated with sample at room temperature for 1 hour. Secondary antibodies are washed off using 3x PBS washes for 10 minutes each. Sample is incubated with Vectashield with DAPI for 5 minutes before coverslip is applied. Nail polish is used to bind the coverslip to the slide for imaging via an inverted confocal microscope.

Slides were imaged using a Leica TCS SP8 inverted confocal microscope, and images were processed and analyzed using ImageJ. Secondary antibody only negative controls can be seen in **Supplemental Figure 1**.

2.10 Flow Cytometry

2.10.1 Sample Preparation

Tumor samples were incubated at 37^{o}C in 1:100 Collagenase I and 1:1000 DNAse I in Dulbecco's Modified Eagle's Medium for 1 hour. Lymph node and spleen samples were pushed through a 40µm cell strainer, and tumor samples were pushed through a 70µm strainer to achieve a single cell suspension. Red blood cells in spleens were lysed using ACK Lysing Buffer (gibco A10492-01) for 5 minutes at room temperature. Cells were centrifuged at 1500RPM at 4^{o}C for 5 minutes and resuspended in FACS buffer (1% BSA, 0.1% sodium azide in PBS) and supernatant was aspirated. Cells were pushed through an additional 40µm cell strainer to remove clumps, and 10µL of each sample was collected for cell counts.

Samples were centrifuged at 1500RPM at 4^{o}C for 5 minutes and supernatant was aspirated. Cells were resuspended in FACS buffer at 100µL multiplied by the number of antibody panels. One hundred microliter (100µL) aliquots per sample were divided for each antibody panel. Each aliquot was blocked using 1:200 dilution Fc blocker (BD Pharmingen 553142) for 5 minutes at room temperature. Then, antibodies were added at 1:200 dilution per sample for 40 minutes at 4^{o}C (See **Table 1: Flow Cytometry**). Samples were washed in 2mL FACS buffer and centrifuged at 1500RPM at 4^{o}C for 5 minutes. Supernatant was removed and cells were fixed in 2% formalin in FACS buffer. Samples were recorded using a BD FACSCANTO II machine and results were analyzed using FlowJo.

2.10.2 Flow Cytometry Analysis

Cell debris was excluded by gating cells with Forward Scatter Area (FSC-A) by Side Scatter Area (SSC-A). Single cells were gated using Forward Scatter Area by Forward Scatter

Height (FSC-H). Leukocytes were gated using $CD45^+$ gates. Then cells populations were determined using appropriate cell surface markers. Sample gating strategies can be seen in **Supplemental Figures 2, 3, 4**.

2.11 Mouse IgG ELISA

Blood plasma was collected according to **Methods 2.7.3 Mouse plasma isolation**.

Buffers, substrates, and standards were prepared in accordance with the Cayman Chemical Mouse IgG ELISA Kit pre-assay preparation (Cayman Chemical 501240).

100µL of standards or diluted samples were added to wells on the plate in triplicate. A 96-well plate was covered and incubated at room temperature for one hour on an orbital shaker. Wells were emptied and washed four times with wash buffer. After the last wash, plate was inverted onto absorbent paper to remove residual wash buffer. One hundred microliters (100µL) of HRP-Conjugate was added to each well of the plate, covered, and incubated for one hour at room temperature on an orbital shaker. Wells were washed the same as before, and 100µL TMB Substrate Solution was added to each well. Plate was covered and incubated for 10 minutes at room temperature on an orbital shaker. One hundred microliters (100µL) of HRP Stop Solution was added to each well of the plate.

Plate was read at 450nm with a SpectraMAX Plus SoftMax Pro 5 plate reader.

Standard curve was generated by averaging the triplicates for the standards' optical density at 100, 50, 25, 12.5, 6.3, 3.2, 1.6, and 0ng/mL. Sample concentrations were calculated using the trendline equation, then accounting for initial 1:20000 dilution.

Sample Calculation of Plasma IgG Concentration:

$$Optical\ Density\ (OD) = 0.6926$$

$$Trendline\ Equation: OD = 0.0272 * Concentration + 0.1308$$

$$0.6926 = 0.0272 * Concentration + 0.1308$$

$$\frac{0.6926 - 0.1308}{0.0272} = Concentration$$

$$Concentration = 20.65441 \frac{ng}{mL}$$

$$Adjusted\ Concentration\ with\ Dilution = 20.65441 \frac{ng}{mL} * 20000 = 413088.2 \frac{ng}{mL}$$

$$413088.2 \frac{ng}{mL} * \frac{1\mu g}{1000 ng} = 413.0882 \frac{\mu g}{mL}$$

CHAPTER THREE: RESULTS

3.1 Germinal center formation is associated with subcapsular sinus macrophage migration in the tumor-draining lymph node

Metastatic tumor cells and tumor-derived antigens enter the tumor-draining lymph node during lymphatic metastasis. To assess what types of immune cells interact with metastatic tumor cells or tumor-derived antigens in the tumor-draining lymph node, 1.0×10^6 green fluorescent protein (GFP) labeled E0771 (E0771-GFP) breast cancer cells were implanted in the fourth right mammary fat pad in 6-8 week old C57BL/6J female mice. On day 21 (3 weeks) after tumor implantation, or when tumor size reached 1000 mm^3, mice were sacrificed, and tumor-draining inguinal lymph nodes were collected for cryosections and flow cytometry. The contralateral inguinal lymph nodes were collected as a control (non-draining lymph node). Previous students in the lab, using several antibodies to label major cell types in the lymph node, observed that tumor cells were restricted in the subcapsular sinus and tumor derived GFP accumulated with $CD169^+$ subcapsular sinus macrophages and PNA^+ germinal centers. I confirmed these studies by repeating the experiments (**Figure 3.1.1A, B**). Importantly, while the metastatic tumor cells may not always be detected in the tumor-draining lymph node by day 21 after tumor implantation, tumor-derived GFP signal was consistently detected in the germinal center with $CD169^+$ subcapsular sinus macrophages. To further confirm if tumor-derived antigen (GFP) was located in the germinal center, I used GL7, another important marker of germinal center B-cells and confirmed that tumor-derived antigen GFP is co-localized with the germinal center (**Figure 3.1.1C, D**).

To exclude the possibility that the germinal center formation occurs in response to the green fluorescent protein as a foreign antigen, normal (unlabeled) E0771 breast cancer cells were

implanted into 6-8 week old C57BL/6J female mice and the draining and the contralateral inguinal lymph nodes were collected for analysis. Lymph node cryosections were stained with CD169, PNA, and LYVE1 (**Figure 3.1.2**). LYVE1 staining denoted the lymphatic endothelial cells located at the lymph node, as a thin layer of LYVE1 is found at the subcapsular sinus and the enriched LYVE1 showed the medullary sinus. Consistently, the regular E0771 induce germinal centers in the tumor-draining inguinal lymph nodes, but not the contralateral inguinal lymph node (**Figure 3.1.2A, B**). CD169 signal appears to spread from the subcapsular sinus to the germinal center (**Figure 3.1.2C**). These results indicate germinal center formation and $CD169^+$ subcapsular sinus macrophage relocation to the germinal center is not an artifact induced by GFP. Since there is no established marker for E0771 endogenous tumor antigens, I used E0771-GFP tumors to visualize the tumor-derived antigens and their interaction with other cells in the tumor-draining lymph node.

It has recently been reported that $CD169^+$ macrophage density was reduced in the tumor-draining lymph node, but the mechanism remains relatively unclear [50, 52]. Because tumor-draining inguinal lymph nodes are enlarged compared to non-draining inguinal lymph nodes (**Figure 3.1.3A, B**), I suspected that the reduced density of $CD169^+$ macrophages in the subcapsular sinus was because $CD169^+$ macrophages relocate to the germinal center. Using flow cytometry analysis, I determined the proportion of subcapsular sinus macrophages ($CD169^+F4/80^-$) was reduced within the lymph node (**Figure 3.1.3C**), but the total number of $CD169^+F4/80^-$ cells did not change (**Figure 3.1.3D**). These results suggest these macrophages were not depleted during tumor growth (**Figure 3.1.3D**). Instead, it appears that the tumor-draining lymph node expands and the subcapsular sinus macrophages are not replicating to adjust for the increased size and surface area of the lymph node capsule. Staining a naïve lymph

node capsule with Collagen I (red) demonstrated the typical layer of macrophages (green) underlying the subcapsular sinus in the lymph node (**Figure 3.1.3E**). In the tumor-draining lymph node, these macrophages appear to depart away from their typical location, and traffic deeper into the lymph node (**Figure 3.1.3F**). Together, these data show that subcapsular sinus macrophages migrate away from the subcapsular sinus, leaving gaps in the subcapsular sinus. Some of these macrophages moved into the germinal center.

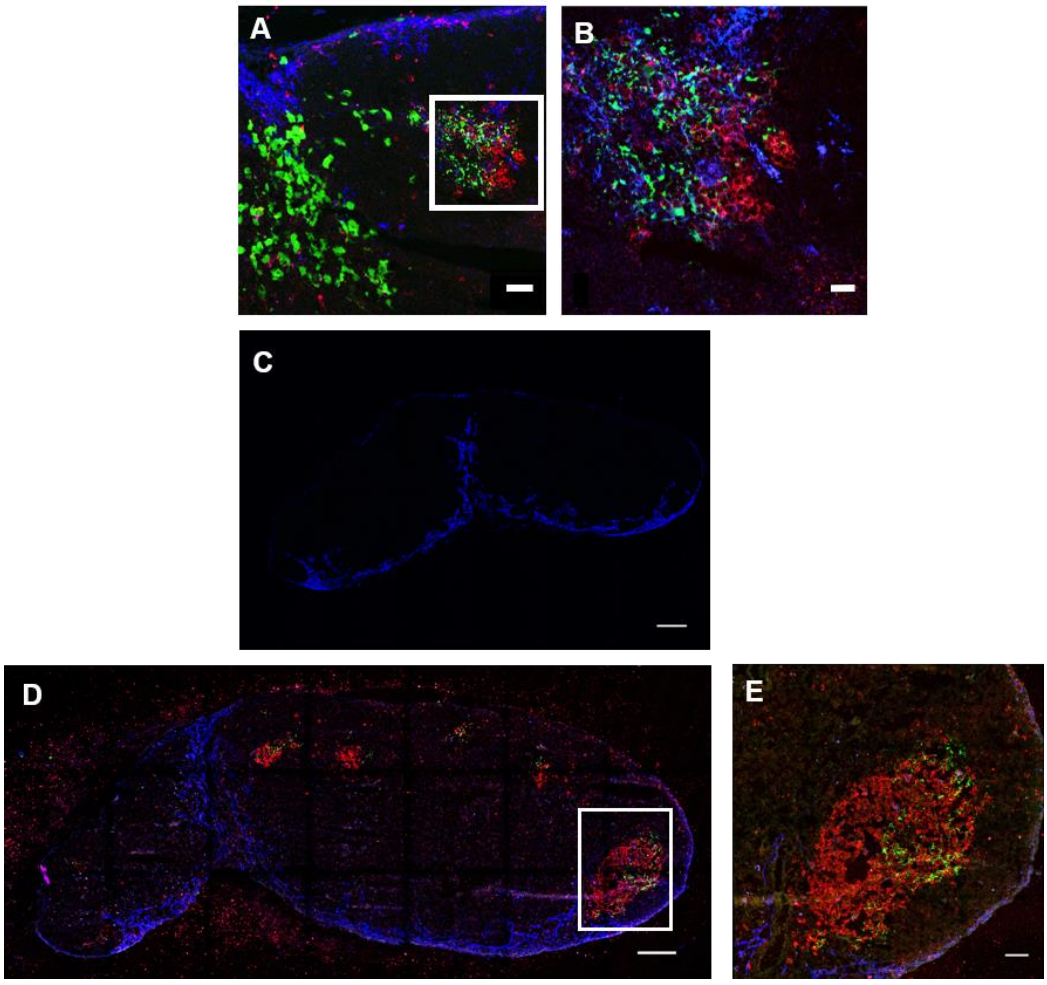

Figure 3.1.1: Tumor-draining lymph node forms germinal center in E0771-GFP tumor-draining lymph node 21 days post-implantation and germinal center colocalizes with subcapsular sinus macrophages and tumor-derived antigens. A, B. Immunofluorescent image of germinal center formation in E0771-GFP tumor-draining lymph node 21 days post-implantation (Scale bar: 50μm, original magnification: 630x). E0771-GFP (green), PNA (red), CD169 (blue). **C.** Immunofluorescent image of E0771-GFP non-draining lymph node 21 days post-implantation (Scale bar: 200μm, original magnification 200x). E0771-GFP (green), GL7 (red), LYVE1 (blue) **D, E.** Immunofluorescent image of germinal center formation in E0771-GFP tumor-draining lymph node 21 days post-implantation (Scale bar: 200μm, original magnification 200x). E0771-GFP (green), GL7 (red), LYVE1 (blue). All images are a representative image of n = 3.

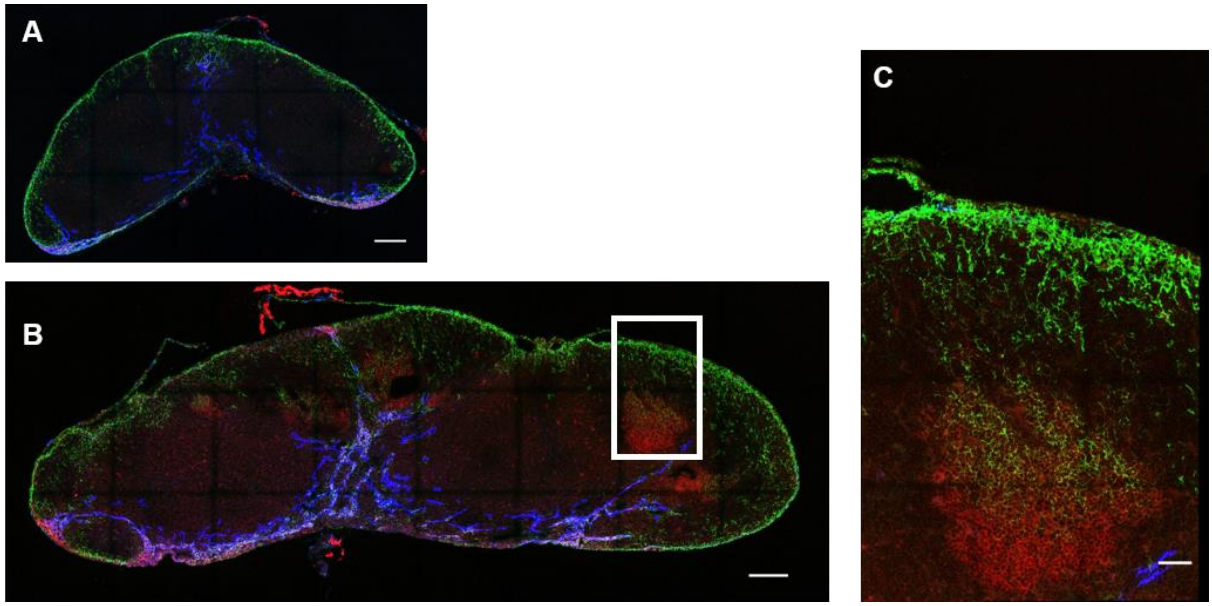

Figure 3.1.2: Tumor-draining lymph node forms germinal center in E0771 tumor-draining lymph node 21 days post-implantation independently of GFP and colocalizes with CD169 signal. A, B. Tile scans of non-draining lymph node and tumor-draining lymph node respectively (Scale bars: 200µm, original magnification 200x). CD169 (green), PNA (red), LYVE1 (blue). **C.** Subcapsular sinus macrophages migrate away from the subcapsular sinus and accumulate with the germinal center B-cells. (Scale bar: 50µm, original magnification 630x). CD169 (green), PNA (red), LYVE1 (blue). All images are a representative image of n = 3.

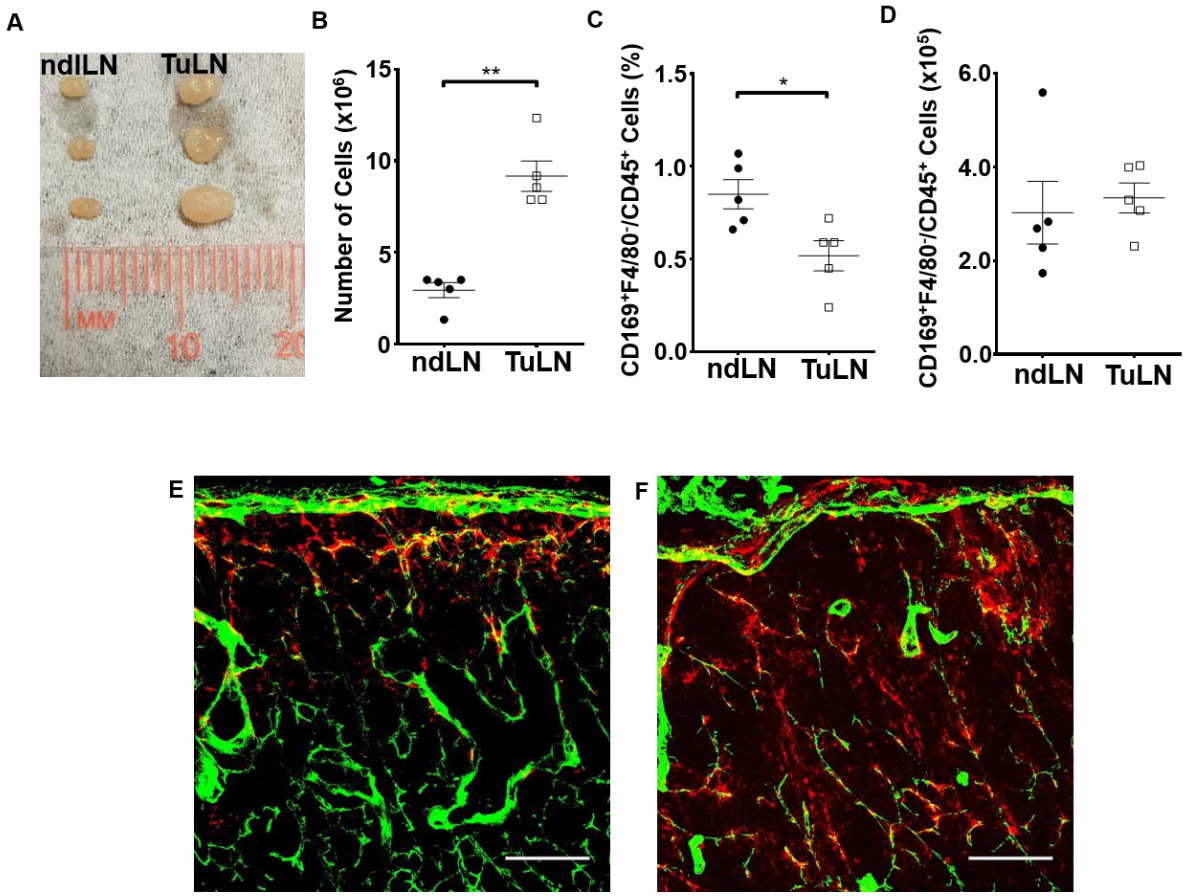

Figure 3.1.3: Tumor-draining lymph nodes have an increased number of cells and CD169$^+$ macrophage layer is disrupted. A. Image of non-draining inguinal lymph node and 21-day E0771 tumor-draining lymph node. **B**. Total cell counts of non-draining inguinal lymph node and 21-day E0771 tumor-draining lymph node (n=5 per group, repeated twice). Data is mean ± SEM. **P<0.01. Mann-Whitney U test. **C**. Flow cytometry analysis of CD169$^+$F4/80$^-$ (SCS) macrophages in non-draining inguinal lymph nodes and 21-day E0771 tumor-draining lymph nodes (n=5 per group, repeated twice). Data is mean ± SEM. *P<0.05. Unpaired, parametric student's t-test. **D**. Number of CD169$^+$F4/80$^-$ cells in non-draining inguinal lymph node and 21-day E0771 tumor-draining lymph node (n=5 per group, repeated twice). Data is mean ± SEM. Mann-Whitney U test. **E, F.** Immunofluorescent images of non-draining lymph node and tumor-draining lymph node subcapsular sinus macrophages and the lymph node capsule respectively (Scale bar: 50µm, original magnification: 630x). Collagen I (green), CD169 (red). Images are a representative of n = 3.

3.2 Reduced E0771 tumor growth in B-cell deficient mice

Germinal center formation suggested B-cells are activated in the tumor-draining lymph node. To determine if germinal center formation is only a consequence of tumor growth or if B-cell activation is actively involved in regulating tumor growth, I implanted E0771 tumor cells into B-cell deficient mice (μMT mouse model) to compare tumor growth with wild-type mice. Homozygous μMT mutant mice lack mature B-cells as there is a stop codon preventing the μ exon from transcribing the μ heavy chain. The μ heavy chain is an important component of the membrane-bound IgM complex on pre-B-cells. Without membrane-bound IgM, pre-B-cell differentiation and maturation does not occur, arresting the production of mature B-cells [53]. Over 21 days, μMT mice show significantly less tumor growth compared to their wild-type C57BL/6J controls (**Figure 3.2.1A**). Therefore, B-cells promote E0771 breast cancer tumor growth in mice.

Wild-type and μMT tumor-draining lymph nodes were collected on day 21 and stained for Collagen I and PNA to assess germinal center formation (**Figure 3.2.1B, C**). Consistent with previous studies, wild-type mice show PNA^+ germinal centers and GFP accumulation (**Figure 3.2.1B, D**), and as expected, there is no germinal center formation in the μMT tumor-draining lymph node (**Figure 3.2.1C**). Additionally, B-cell deficient E0771-GFP tumor-draining lymph nodes lack tumor-derived antigen accumulation when germinal centers are not present (**Figure 3.2.1E**). Thus, tumor-derived antigen accumulation in the lymph node also depends on B-cells.

In summary, E0771 tumor growth is suppressed in B-cell deficient mice, which is consistent with the previously reported B16F10 melanoma model [50]. Our studies further confirmed that B-cell activation in the tumor-draining lymph node is associated with enhanced tumor growth.

Next, I aimed to determine if transferring wild-type B-cells back into the μMT mice was enough to induce tumor growth. I isolated B-cells from the spleens of C57BL/6 wild-type mice using the MACS separation method and labeled them with CFSE. The purity of the isolated B cells was approximately 90% by FACS (**Figure 3.2.2)**. To determine the quantity of B-cells recovered in inguinal lymph nodes after transplantation, I transferred 10 x 10^6, 15 x 10^6, or 20 x 10^6 C57BL/6 B-cells to μMT mice. Inguinal lymph nodes were collected 2 weeks later, and B cell population was detected using flow cytometry. Only a small population of B-cells was restored in the μMT mice lymph nodes when transferred with 15 x 10^6 B cells (**Figure 3.2.2**). In wild-type mice, $CD19^+$ B-cells account for approximately 40% of lymph node $CD45^+$ leukocytes. Comparatively, μMT mice have a negligible proportion of $CD19^+$ cells (0.05%) in the lymph node. After 15 x 10^6 wild-type B-cells are transferred into μMT mice, approximately 0.2% of $CD19^+$ B-cells were recovered in the inguinal lymph node after 14 days. There was no significant improvement when transferred with 20 x 10^6 B cells (**data not shown**).

To determine if a small proportion of B-cell reconstruction in μMT mice can recover tumor growth, 15 x 10^6 purified wild type B-cells were transferred into 6-8 week-old female μMT mice. Two weeks after B-cell transfer, E0771 breast cancer was implanted into the fourth right mammary fat pad. Wild-type and μMT tumor growth curves were consistent with previous experiments, with μMT E0771 tumors growing significantly less compared to wild-type E0771 tumors. In μMT mice with B-cell transfer, E0771 tumor growth is restored back to wild-type levels. This indicates that transferred B-cells are enough to restore tumor growth (**Figure 3.2.3A**). The tumor-draining lymph nodes were stained for Collagen I, PNA, and CD45R/B220 (**Figure 3.2.3B**, **C**). B220 staining pattern shows minimal B-cell recovery in the lymph node B-cell follicles, consistent with the quantitative flow cytometry data (**Figure 3.2.2**). There was no

PNA staining detected in the μMT mice with B-cell transfer, nor were there any traces of GFP signal (**Figure 3.2.3C, E**). These results suggested that B-cells are necessary for E0771 tumor growth, but germinal center formation is not. This also demonstrates the necessity of germinal centers for tumor-derived antigen accumulation.

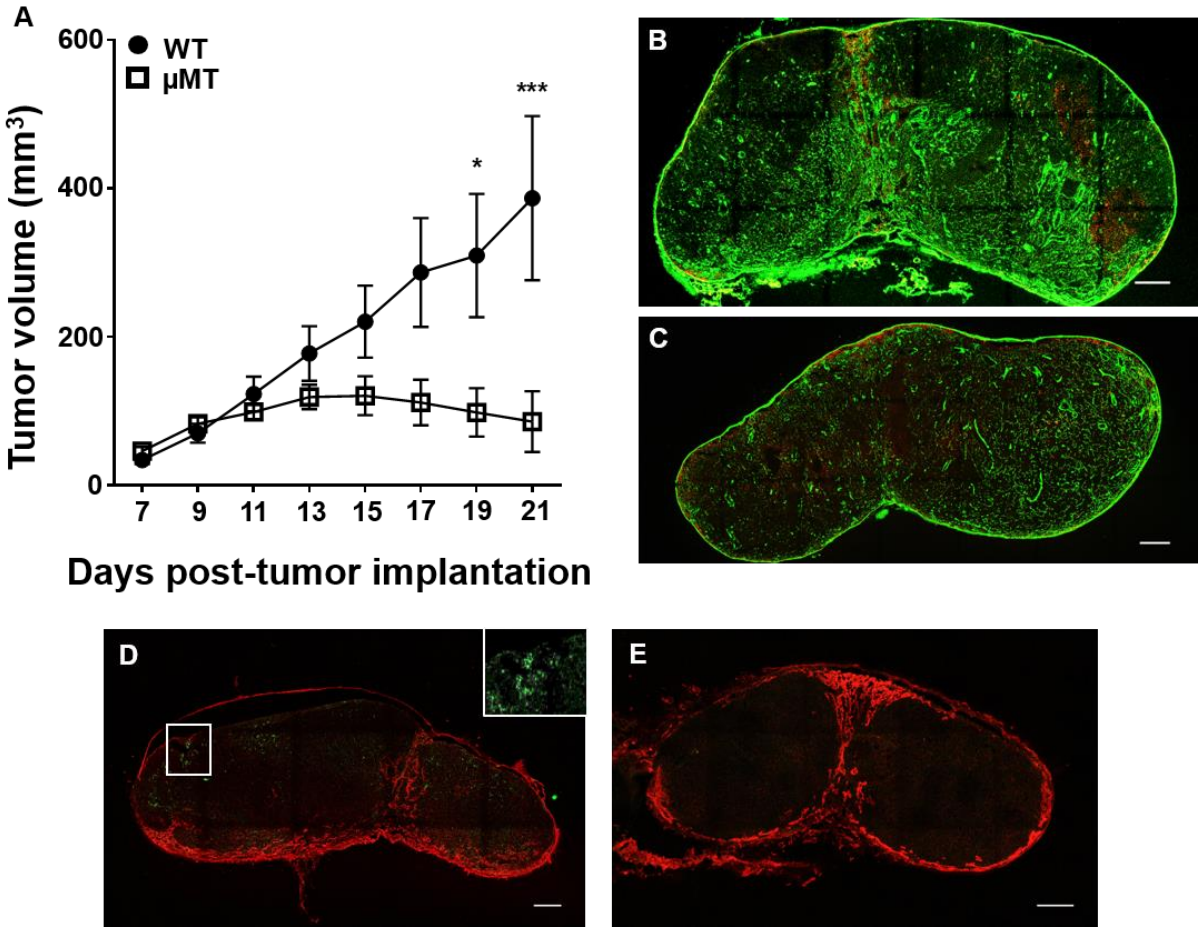

Figure 3.2.1: B-cell deficient mice (μMT) show significantly less tumor growth compared to C57BL/6 wild-type. B-cell deficient mice do not form germinal centers nor accumulate tumor-derived antigens in the tumor-draining lymph node. A. E0771 tumor growth curve of a C57BL/6 wild-type mouse compared to a μMT mouse over 21 days. (n=5-10 per group, repeated twice). Data is mean ± SEM. *P<0.05, ***P<0.001. Two-way ANOVA with Sidak's multiple comparisons test. **B, C.** Tile scans of C57BL/6 wild-type and μMT 21d E0771 tumor-draining lymph nodes respectively (Scale bar: 200μm, original magnification 200x). Collagen I (green), PNA (red). **D, E.** Tile scans of C57BL/6 wild-type and μMT 21d E0771-GFP tumor-draining lymph nodes respectively (Scale bar: 200μm, original magnification 200x). GFP (green), LYVE1 (red). All images are a representative image of n = 3.

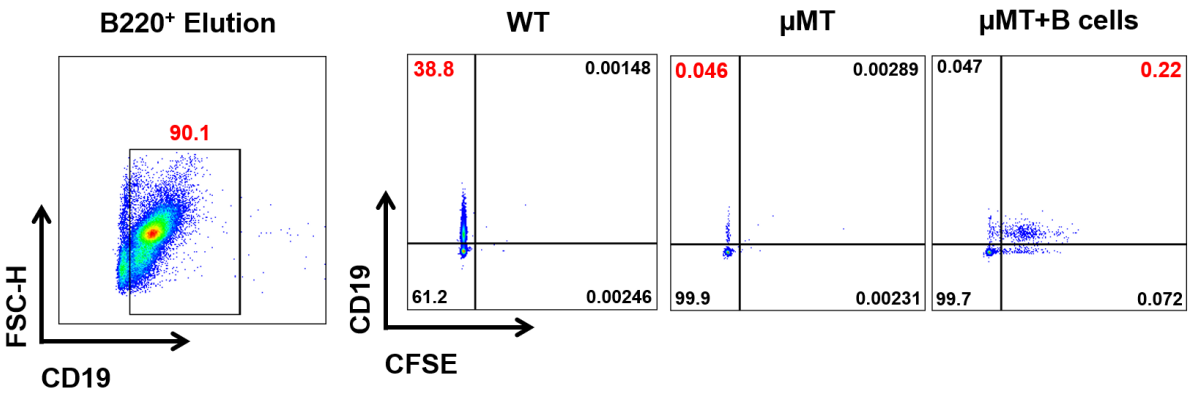

Figure 3.2.2: MACS B-cell isolation yields approximately 90% B220^{+}CD19^{+} cells. Intravenous B-cell transfer recovers a small proportion of inguinal lymph node B-cells over 2 weeks. Representative flow dot plots of CD19^{+} B-cells after MACS isolation and after transfer into in wild-type, μMT, and μMT mice two weeks post-CFSE-labeled B-cell transfer (n = 3, repeated thrice).

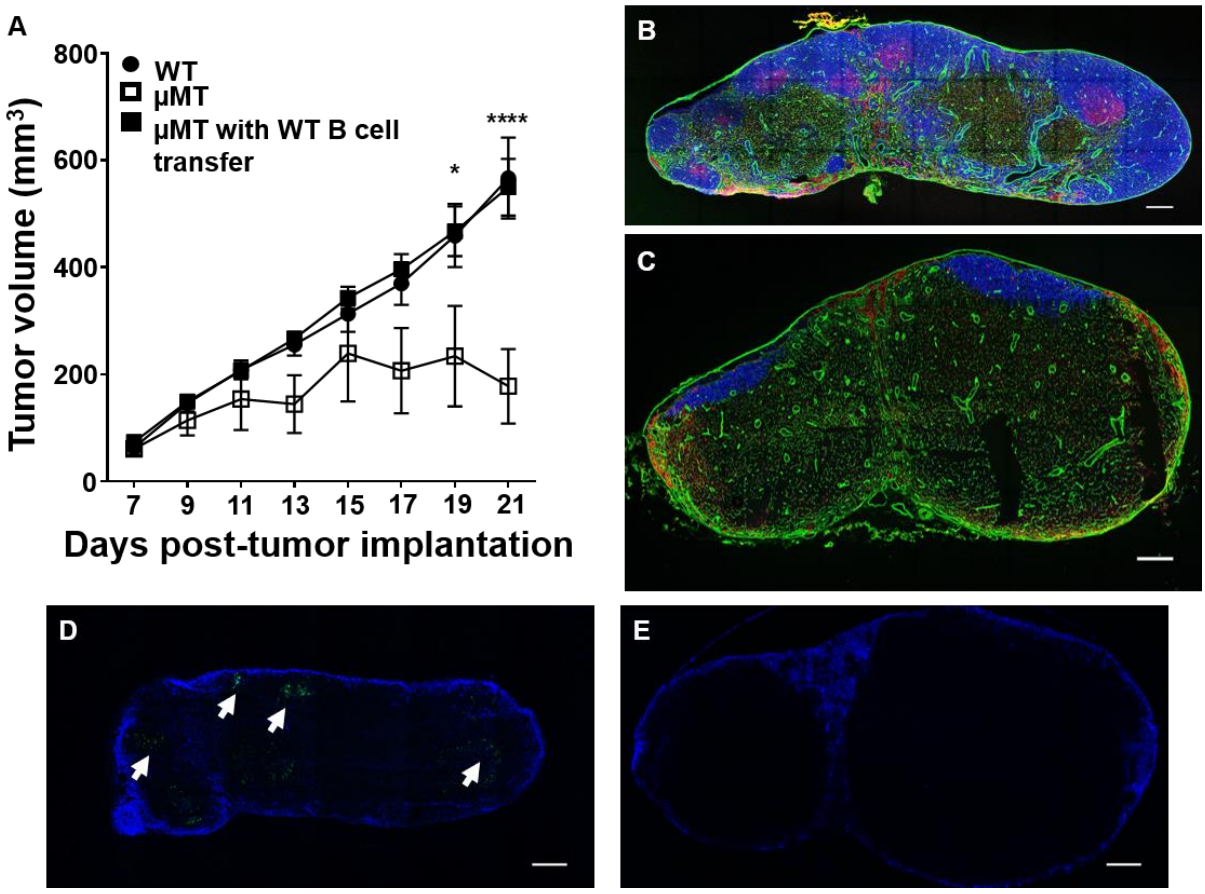

Figure 3.2.3: B-cell transfer into µMT mice recovers tumor growth to C57BL/6 wild-type levels but does not recover germinal center formation nor tumor-derived antigen accumulation in the tumor-draining lymph nodes. A. E0771 tumor growth curve of C57BL/6 mice, µMT mice, and µMT mice with wild-type mice B-cells over 21 days. (n=5-10 per group, repeated twice). Data is mean ± SEM. *P<0.05, ****P<0.0001. Two-way ANOVA with Sidak's multiple comparisons test. **B, C.** Tile scans of C57BL/6 wild-type and µMT with C57BL/6 B-cells 21d E0771 tumor-draining lymph nodes respectively (Scale bar: 200µm, original magnification 200x). Collagen I (green), B220 (blue), PNA (red). **D, E.** Tile scan of wild-type and B-cell recipient µMT E0771-GFP tumor-draining lymph node (Scale bar: 200µm, original magnification 200x). GFP (green, white arrows), CD169 (blue). All images are a representative of n = 3.

3.3 Single plasma transfer is not enough to restore tumor growth

Because germinal center formation implies the production of high affinity antibodies against the tumor, I looked to determine if antibodies produced in the E0771 tumor-bearing wild-type blood plasma accelerates tumor growth. Mouse IgG ELISA were conducted on control wild-type, and E0771 tumor-bearing wild-type, µMT, and B-cell recipient µMT mice blood plasma (**Figure 3.3.1A**). Without a tumor, control wild-type mice have approximately 300µg/mL plasma IgG. E0771 tumor-bearing wild-type mice have significantly higher plasma IgG, at approximately 400µg/mL, indicating B-cell activation in tumor-bearing mice. In contrast, E0771 tumor-bearing µMT mice show minimal plasma IgG, suggesting a deficiency in the µ-heavy chain significantly depletes IgG production. Finally, B-cell transfer into µMT does not significantly recover plasma IgG levels in tumor-bearing mice, suggesting plasma IgG is not correlated with increased tumor growth**.**

To confirm this observation, tumor-bearing wild-type plasma and µMT plasma were intravenously injected into wild-type mice alongside an E0771 tumor implantation. Tumor growth was observed over 21 days (**Figure 3.3.1B**). Tumor growth of wild-type mice receiving wild-type or µMT plasma did not significantly deviate from normal wild-type E0771 tumors. This suggests tumor-induced plasma IgG does not accelerate tumor growth. Alternatively, it is possible that the effect of IgG plateaus in wild-type mice, and additional IgG did not cause further enhancement of tumor growth, thus showing minimal influence when external plasma is introduced to wild-type tumor growth. To exclude this possibility, tumor-bearing wild-type plasma was intravenously transferred alongside with E0771 tumor implantation into µMT mice. Wild-type plasma µMT recipients show similar tumor growth compared to E0771 tumor-bearing µMT mice – significantly slower compared to E0771 tumor-bearing wild-type mice (**Figure**

3.3.1C). Cumulatively, these data suggest a one-time plasma transfer is not enough to increase tumor growth. Coupled with the B-cell transfer data, it appears that the necessity for B-cells in E0771 tumor growth most likely depends on B-cells rather than plasma IgG.

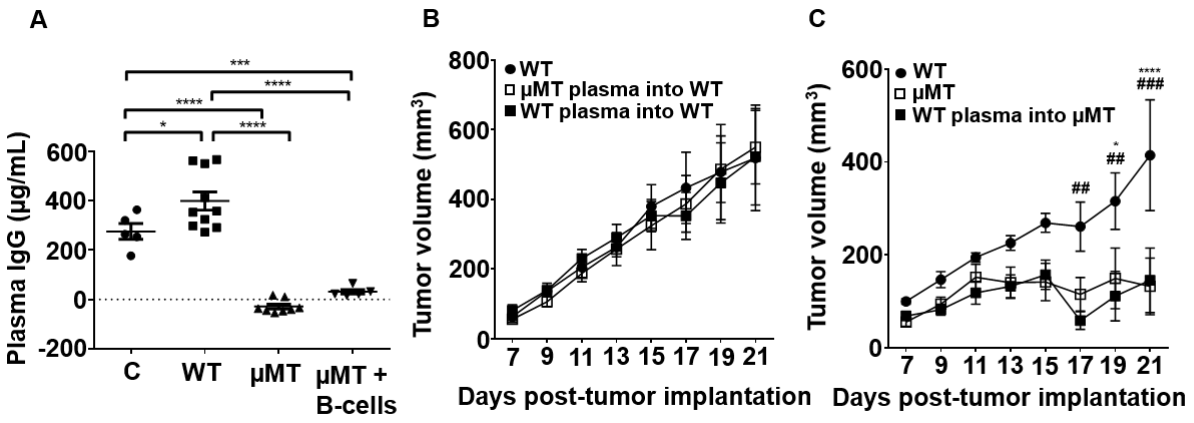

Figure 3.3.1: One-time plasma transfer from an E0771 tumor-bearing mouse does not affect the growth rate of C57BL/6 wild-type tumors nor µMT tumors. A. Plasma IgG levels in wild-type control (C), E0771 tumor-bearing wild-type, µMT and µMT with wild-type B-cells (n=5-10 per group, repeated twice). Data is mean ± SEM. *P<0.05, ***P<0.001, ****P<0.0001. One-way ANOVA with Tukey's multiple comparisons test. **B.** E0771 growth curve of WT, WT with tumor-bearing µMT plasma, and WT with tumor-bearing WT plasma (n=5-10 per group, repeated twice). Data is mean ± SEM. Two-way ANOVA with Sidak's multiple comparisons test. **C.** E0771 growth curve of WT, µMT, and µMT with WT tumor-bearing plasma (n=5-10 per group, repeated twice). Data is mean ± SEM. *P<0.05, **P<0.01, ***P<0.001, ****P<0.0001. Two-way ANOVA with Sidak's multiple comparisons test.

3.4 μMT mice lack a subcapsular sinus macrophage layer and B-cell transfer recovers this phenotype

It has been previously documented that μMT mice lack the subcapsular sinus macrophages phenotype ($CD169^{+}F4/80^{-}$) [31]. It is possible that these subcapsular sinus macrophages are required to direct tumor-derived antigens into the B-cell zone or to stimulate the formation of germinal centers. To address this question, we first conducted flow cytometry on the lymph nodes of wild-type and μMT mice. I assessed two major different lymph node macrophage phenotypes: subcapsular sinus macrophages ($CD169^{+}F4/80^{-}$) and medullary sinus macrophages ($CD169^{low}F4/80^{+}$ and $CD169^{-}F4/80^{+}$). As expected, the proportion of subcapsular sinus macrophage phenotype ($CD169^{+}F4/80^{-}$) was significantly smaller in the μMT mice compared to wild-type mice. Consistent with the literature, the medullary sinus macrophage phenotype was the dominant population as $CD169^{low/-}F4/80^{+}$ proportions increased in μMT mice (**Figure 3.4.1A**).

After reaffirming that μMT mice lack the subcapsular sinus macrophage phenotype, I used immunofluorescent staining to determine if B-cell transfer recovers this cell population. First, I stained μMT control lymph nodes and CFSE-labeled B-cell recipient μMT lymph nodes with LYVE1 and CD169 to determine the restoration of subcapsular sinus macrophages (**Figure 3.4.1B, C**). CFSE signaling shows B-cells localize underneath the subcapsular sinus in the μMT lymph node after B-cell transfer. Furthermore, $CD169^{+}$ signaling can be seen at the subcapsular sinus after B-cell transfer, while μMT control mice show no $CD169^{+}$ signal. Then, I stained E0771-tumor bearing wild-type, μMT, and B-cell recipient μMT mice with Collagen I, PNA, and CD169. Wild-type and μMT E0771 tumor-draining lymph nodes remain consistent with previous experiments; wild-type tumor-draining lymph nodes form germinal centers and subcapsular sinus

macrophages are colocalized with them (**Figure 3.4.1D**). μMT tumor-draining lymph nodes show no germinal center formation and no typical subcapsular sinus macrophage layer (**Figure 3.4.1E**). B-cell recipient μMT mice show a recovered $CD169^+$ subcapsular sinus layer, but no germinal center formation (**Figure 3.4.1F**). Thus, the transfer of B-cells can recover the subcapsular sinus macrophage layer, but not germinal center formation.

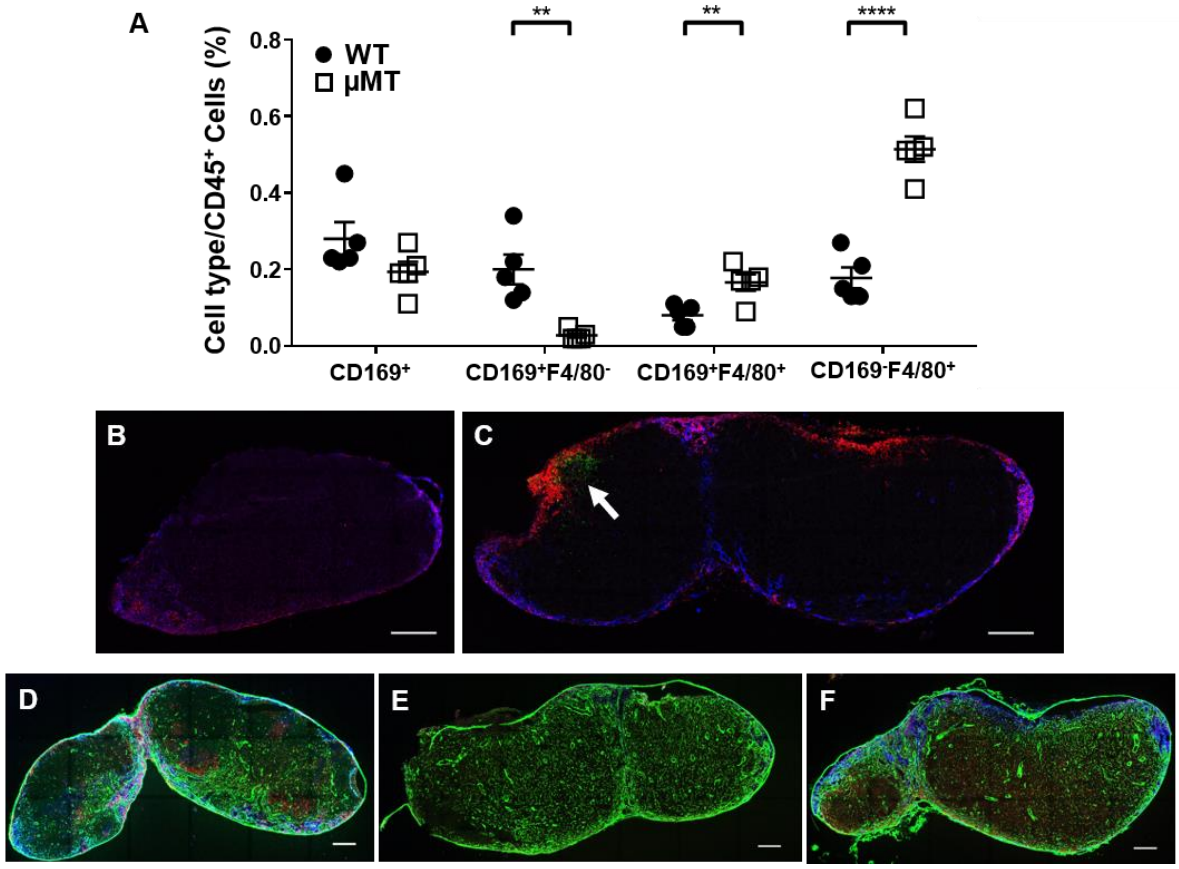

Figure 3.4.1: µMT mice have a lower proportion of the subcapsular sinus macrophage phenotype and a higher proportion of medullary sinus macrophage phenotype. Wild-type B-cell transfer recovers the subcapsular sinus macrophage phenotype. A. Flow cytometry on C57BL/6 wild-type and µMT lymph nodes. (n=5 per group, repeated twice). Data is mean ± SEM. **P<0.01, ****P<0.0001. Multiple unpaired t-tests. **B, C.** Tile scans of µMT and B-cell recipient µMT inguinal lymph nodes 14 days post-B-cell transfer (scale bar: 200µm, original magnification: 200x). CFSE (green, arrow), CD169 (red), LYVE1 (blue). **D, E, F.** Tile scans of 21d E0771 C57BL/6, µMT, and µMT with C57BL/6 wild-type B-cell transfer tumor-draining lymph nodes respectively (scale bar: 200µm, original magnification 200x). Collagen I (green), PNA (red), CD169 (blue). All images are a representative image of n = 3.

3.5 Depletion of lymph node subcapsular sinus macrophages enhances germinal center formation, tumor antigen accumulation, and significantly accelerates tumor growth

So far, I have shown that transferring B-cells can recover tumor growth, but a single plasma transfer cannot. However, transferring B-cells into μMT mice did not recover germinal centers, but recovers subcapsular sinus macrophages. In wild-type mice, CD169 macrophages dissociate from the SCS and accumulated with tumor antigens in the germinal center in the tumor-draining lymph node (**Figure 3.1.1**). It is possible that reconstruction of B-cells restores $CD169^+$ macrophages to enhance tumor growth. To test this possibility, we utilized a clodronate liposome model, which is commonly used in studies involving the depletion of subcapsular sinus macrophages.

To establish a proper method to deplete $CD169^+$ subcapsular sinus macrophages with clodronate liposomes, I intradermally injected clodronate liposomes into the hind flank above the targeted inguinal lymph node. I conducted several control experiments to confirm the effects of clodronate liposomes. A treatment of 50μL clodronate liposome intradermal flank injection specifically depleted the subcapsular sinus macrophages ($CD169^+F4/80^-$) in the draining lymph node 7 days post-injection. This is visualized in lymph node cryosections stained for CD169 and LYVE1, as draining lymph nodes show no $CD169^+$ signal along the subcapsular sinus (**Figure 3.5.1A, B**). This is quantitatively confirmed with flow cytometry as the clodronate liposome-draining lymph node $CD169^+F4/80^-$ cells were significantly depleted, but all other macrophage types remained at normal proportions compared to PBS liposome controls (**Figure 3.5.1E**). I further determined the recovery rate of the subcapsular sinus macrophages after depletion. The subcapsular sinus macrophages were recovered 14 days post-intradermal injection, visualized in cryosections (**Figure 3.5.1C, D**) and quantified by flow cytometry (**Figure 3.5.1F**). Clodronate

liposome-treated lymph nodes cryosections showed similar $CD169^+$ signal along the subcapsular sinus as the PBS liposome group 14-days-post-injection, and cell population analysis on the lymph node macrophage populations showed no significant differences between either group. Additionally, I analyzed the non-draining inguinal lymph node and the spleen to assess the effect of intradermal clodronate liposome injection on subsequent lymph nodes and distant organs respectively. In my flow cytometry analysis, I found no depletion of the macrophage cell populations in the non-draining lymph or the spleen, suggesting the intradermal flank injection only locally depletes the lymph node subcapsular sinus macrophages (**Figure 3.5.2**). These results defined my methods for the next set of experiments.

With an established method of specifically depleting subcapsular sinus macrophages, I implanted E0771-GFP tumors into clodronate liposome-treated mice. To ensure my clodronate liposome treatment did not affect tumor populations, I ran flow cytometry on the tumors. There were no significant differences in the tested macrophage populations in the tumor (**Figure 3.5.3**). Consistent with published literature, the local depletion of lymph node subcapsular sinus macrophages significantly accelerated tumor growth (**Figure 3.5.4A**). This suggests subcapsular sinus macrophages suppress E0771 tumor growth.

I further looked at the tumor-draining lymph node to elucidate tumor antigen accumulation and germinal center formation in these mice. Staining PBS liposome and clodronate liposome-treated E0771-GFP tumor-draining lymph node cryosections allowed us to visualize germinal center formation. Using GL7 and LYVE1, I determined germinal center formation in both PBS liposome and clodronate liposome-treated lymph nodes (**Figure 3.5.4B, C**). Therefore, subcapsular sinus macrophages are not necessary for germinal center formation.

As germinal center formation occurred in both PBS liposome and clodronate liposome-treated tumor-draining lymph nodes, I determined if subcapsular sinus macrophages play any role in germinal center formation or structure. Cryosections of the germinal centers stained for CD169 and PNA show germinal center formation remains consistent between PBS liposome and clodronate liposome-treated tumor-draining lymph nodes, with the exception of CD169 signal (**Figure 3.5.5A, B**). GFP signal from the E0771-GFP tumor also remains similar. Thus, tumor-derived antigen in the germinal center did not depend on subcapsular sinus macrophages.

Visually, germinal center structure is not affected by subcapsular sinus macrophage presence. While individual germinal centers appear similar, I assessed germinal center formation in the whole lymph node. Using cryosections of the treated tumor-draining lymph nodes, I counted the number of germinal centers present and measured their diameters. Per lymph node, germinal center count was higher in the clodronate liposome-treated group compared to the PBS liposome-treated group (**Figure 3.5.5C**), while the average diameter of each group was similar (**Figure 3.5.5D**). Based on image analysis of these cryosections, subcapsular sinus macrophages suppressed germinal center formation.

As there are more germinal centers in clodronate liposome-treated mice, I conducted mouse IgG ELISAs on PBS liposome and clodronate liposome-treated E0771 tumor-bearing mice to determine if subcapsular sinus macrophages regulate IgG production. Plasma IgG levels are similar between PBS and clodronate liposome groups, suggesting an increased number of germinal center formation does not produce more plasma IgG (**Figure 3.5.5E**).

Together, these results show that depleting subcapsular sinus macrophages accelerates tumor growth and is associated with increased germinal center formation in the tumor-draining lymph node. However, it does not appear that the concentration of plasma IgG is the cause of the

increased tumor growth. Therefore, the role of $CD169^+$ macrophages in the germinal center is more likely to prevent B-cell activation.

Finally, it is possible that the local clodronate liposome treatment might indirectly impact macrophages in other organs or in the tumor and cause a systemic effect that influences tumor growth. To exclude this possibility, I intraperitoneally injected clodronate liposomes and quantified macrophage populations in the lymph node and spleens (**Figure 3.5.6A**). Intraperitoneal injection of clodronate liposomes affects both lymph nodes and spleens, depleting macrophage subsets in both. In the lymph node, subcapsular sinus macrophages ($CD169^+F4/80^-$) are depleted. In the spleen, $CD169^+F4/80^+$ macrophages are depleted. Then, I tested the E0771 tumor growth in systemic macrophage-depleted mice. Interestingly, systemically depleting macrophages did not affect tumor growth as both PBS liposome and clodronate liposome-treated groups showed similar tumor growths (**Figure 3.5.6B**). This confirms systemic macrophage depletion did not enhance tumor growth, which is different from the local lymph node subcapsular sinus macrophage depletion.

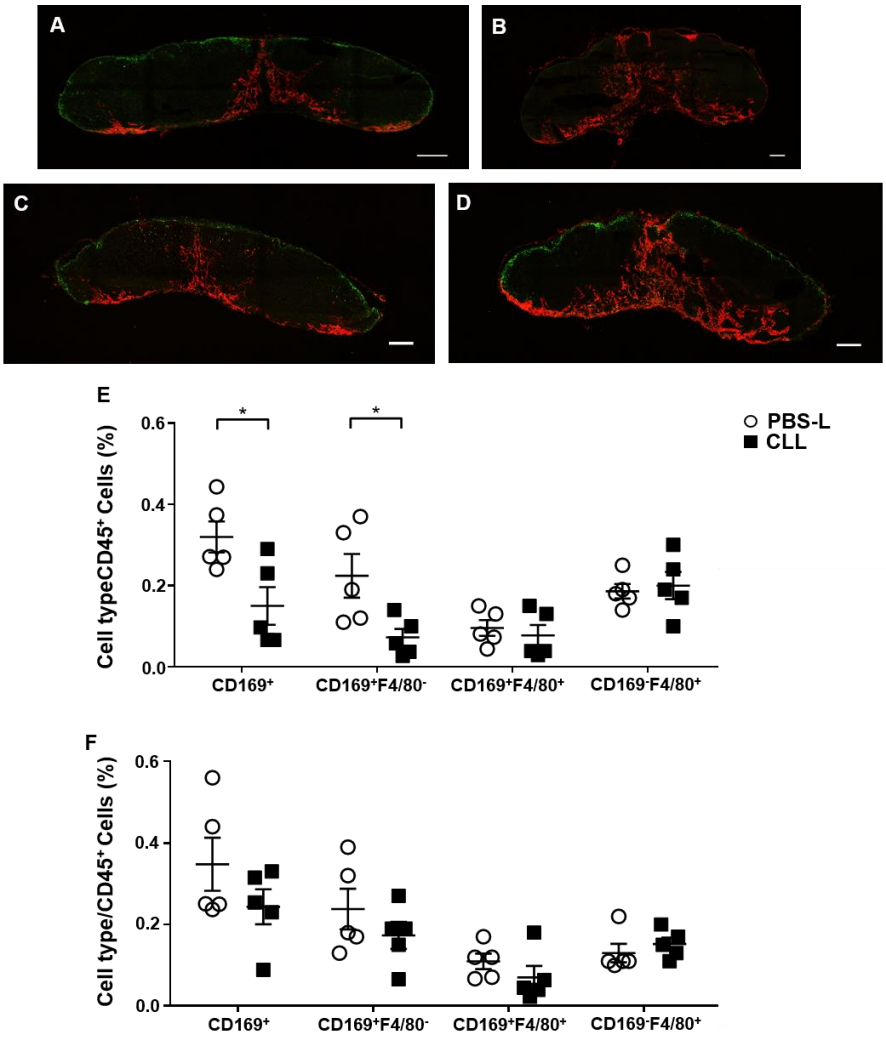

Figure 3.5.1: Subcapsular sinus macrophages are depleted 7 days post-clodronate liposome local flank injection and are recovered 14 days post-clodronate liposome treatment. Other macrophage subsets are not depleted. A, B. Tile scan of PBS liposome and clodronate liposome-treated draining lymph nodes 7 days post-intradermal injection respectively (scale bar: 200μm, original magnification 200x). CD169 (green), LYVE1 (red). **C, D.** Tile scan of PBS liposome and clodronate liposome-treated draining lymph nodes 14 days post-intradermal injection respectively (scale bar: 200μm, original magnification 200x). CD169 (green), LYVE1 (red). **E.** Flow cytometry analysis of PBS liposome and clodronate liposome-treated draining lymph node 7 days post-intradermal injection (n=5 per group, repeated twice). Data is mean ± SEM. *P<0.05. Multiple unpaired, parametric student's t-test. **F**. Flow cytometry analysis of PBS liposome and clodronate liposome-treated draining lymph node 14 days post-intradermal injection (n=5 per group, repeated twice). Data is mean ± SEM. Multiple unpaired, parametric student's t-test. All images are a representative of n = 3.

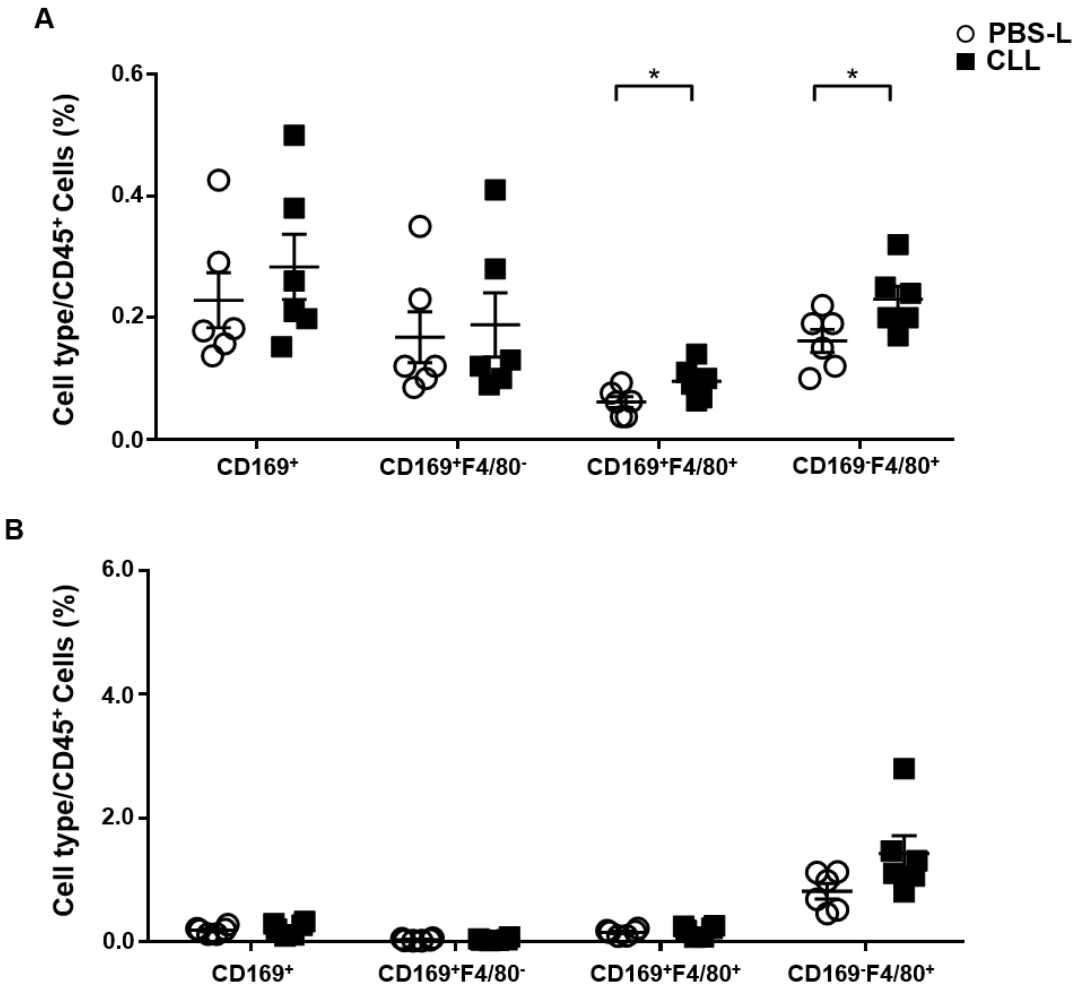

Figure 3.5.2: Intradermal flank clodronate liposome treatment does not any deplete macrophages in the non-draining lymph node nor the spleen. A. Flow cytometry analysis of the contralateral inguinal lymph node 7 days post-intradermal flank PBS liposome or clodronate liposome treatment (n=6 per group, repeated twice). Data is mean ± SEM. *P<0.05. Unpaired, parametric student's t-test. **B.** Flow cytometry analysis of the spleen 7 days post-intradermal flank PBS liposome or clodronate liposome treatment (n=6 per group, repeated twice). Data is mean ± SEM. Multiple unpaired, parametric student's t-test.

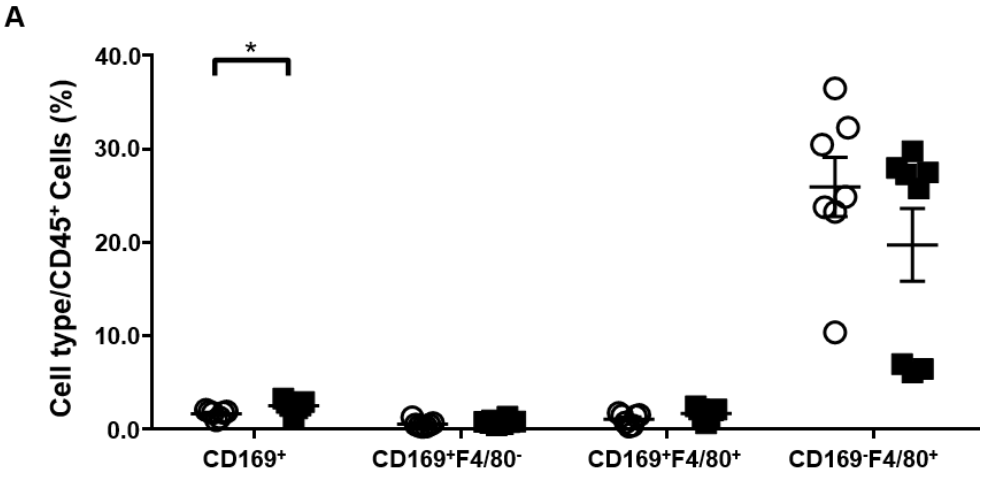

Figure 3.5.3: Intradermal flank clodronate liposome treatment does not deplete macrophages in the tumor. A. Flow cytometry analysis of the tumor 21 days after E0771 tumor implantation in a PBS liposome or CLL-treated mouse (n=7-8 per group, repeated twice). Data is mean ± SEM. *P<0.05. Multiple unpaired, parametric student's t-test.

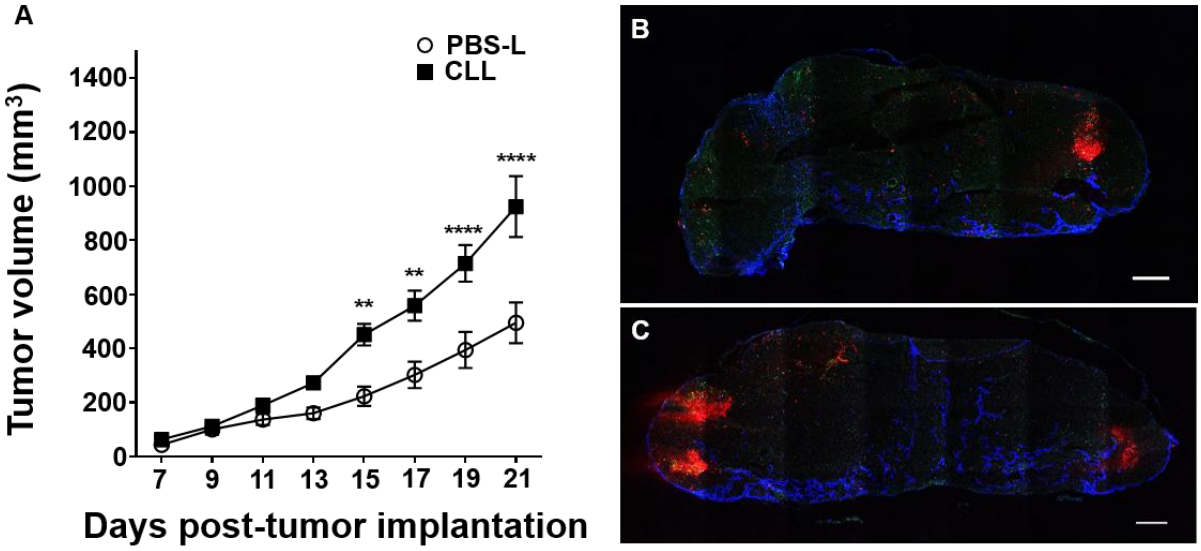

Figure 3.5.4: Specific depletion of tumor-draining lymph node subcapsular sinus macrophages accelerates E0771 tumor growth and germinal centers are formed independently of subcapsular sinus macrophages. A. E0771 growth curve over 21 days of C57BL/6 wild-type mice treated with flank intradermal injection of 50µL PBS liposomes and clodronate liposomes (n=5-10 per group, repeated twice). Data is mean ± SEM. **P<0.01, ****P<0.0001. Two-way ANOVA with Sidak's multiple comparisons test. **B, C.** Tile scans of 21d E0771-GFP tumor-draining lymph nodes treated with PBS liposomes or clodronate liposomes respectively (scale bar: 200µm, original magnification 200x). GFP (green), GL7 (red), LYVE1 (blue). Images are a representative of n = 3.

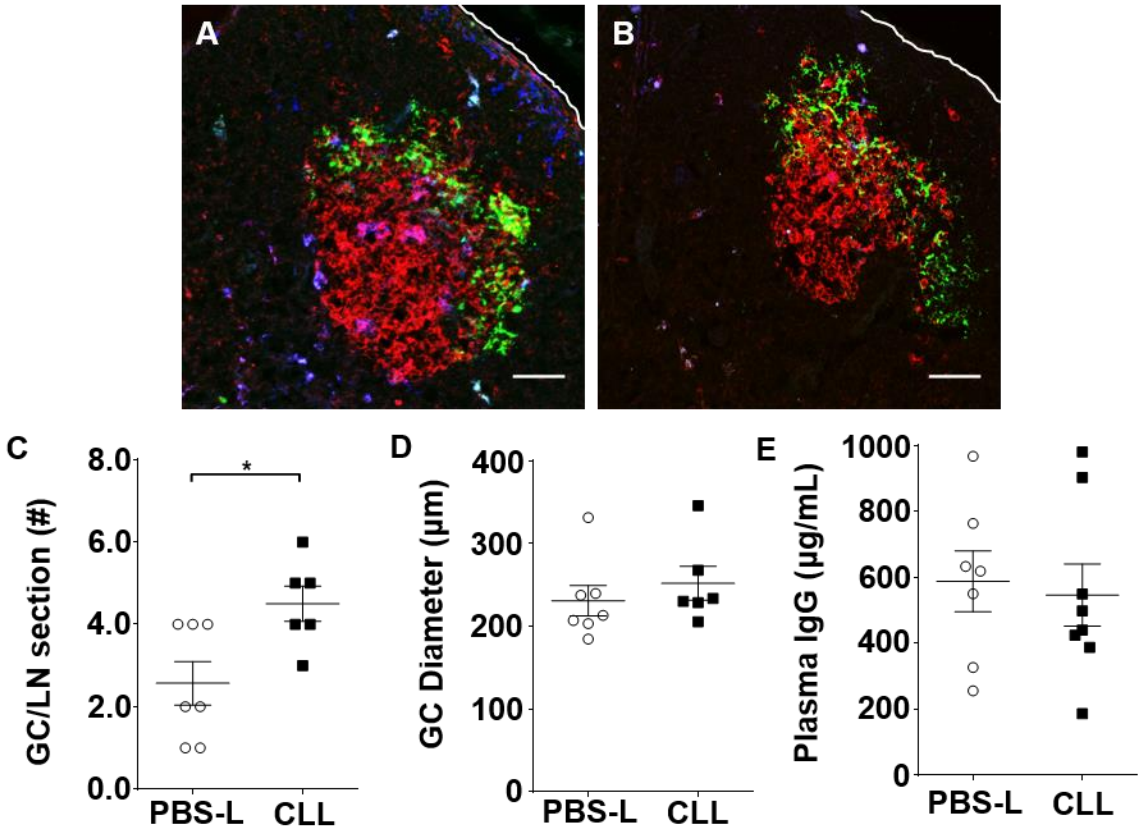

Figure 3.5.5: Tumor-draining lymph node subcapsular sinus macrophage depletion via clodronate liposomes increases number of germinal centers per tumor-draining lymph node but does not affect size nor plasma IgG. A, B. Germinal center images in 21d E0771-GFP tumor-draining lymph nodes treated with PBS liposomes or clodronate liposomes respectively (scale bar: 50µm, original magnification 630x). GFP (green), CD169 (blue), PNA (red). Images are a representative of n = 3. **C.** Germinal center count per tumor-draining lymph node (n=6-7 per group, repeated twice). Data is mean ± SEM. *P<0.05. Mann-Whitney U test. **D.** Average germinal center diameter per lymph node (n=6-7 per group, repeated twice). Data is mean ± SEM. Mann-Whitney U test. **E.** Plasma IgG levels of PBS liposome and clodronate liposome-treated E0771 tumor-bearing mice (n=7-8 per group, repeated twice). Data is mean ± SEM. Mann-Whitney U test.

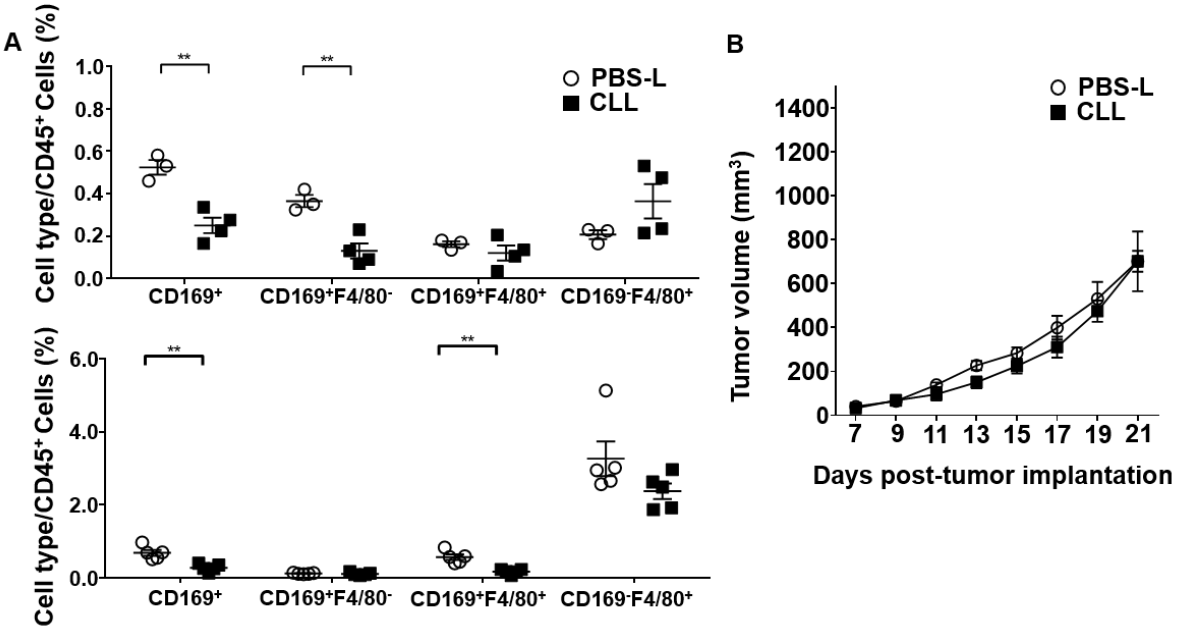

Figure 3.5.6: Intraperitoneal systemic clodronate liposome treatment depletes macrophages in the spleen and the lymph node but does not affect E0771 tumor growth. **A.** Flow cytometry analysis of the PBS liposome and clodronate liposome-treated tumor-draining lymph node and the spleen 21 days post-tumor implantation (n=3-5 per group, repeated twice). Data is mean ± SEM. **P<0.01. Unpaired, parametric student's t-test. **B.** E0771 growth curve over 21 days of C57BL/6 wild-type mice treated with intraperitoneal systemic injection of 150µL PBS liposomes and clodronate liposomes (n=10 per group, repeated twice). Data is mean ± SEM. Two-way ANOVA with Sidak's multiple comparisons test.

CHAPTER FOUR: DISCUSSION

The tumor-draining lymph node is the first secondary lymphoid organ that is directly exposed to tumor-derived antigens and other factors to generate the first wave of immune responses to the growing tumor. Utilizing fluorescent GFP-labeled E0771 tumor cells, an aggregation of tumor-derived antigen (GFP) was found colocalized with $CD169^+$ subcapsular sinus macrophages and germinal centers in the tumor-draining lymph node by day 21 (**Figure 4.1**). Unlabeled E0771 tumors induced germinal center formation and colocalization with $CD169^+$ subcapsular sinus macrophages as well, suggesting this phenomenon is not due to the transgenic GFP. E0771-GFP can serve as the model to observe tumor-derived antigen distribution in the tumor-draining lymph node.

Because $CD169^+$ subcapsular sinus macrophages are dissociated from the subcapsular sinus and some of them relocated to the germinal center, it is possible that $CD169^+$ subcapsular sinus macrophages facilitate tumor antigen accumulation in the germinal center. However, when I depleted this layer of macrophages with clodronate liposomes, tumor growth was accelerated, and additional germinal centers were formed. Thus, $CD169^+$ subcapsular sinus macrophages prevent tumor-derived antigens from entering the B-cell follicle and prevents germinal center formation to suppress tumor growth (**Figure 4.1**). This models the physiological phenomenon as in normal lymph nodes, tumor-derived antigens are typically retained by the subcapsular sinus macrophages. The subcapsular sinus macrophage layer was substantially reduced in the tumor-draining lymph nodes, as the macrophages migrate away from the subcapsular sinus and some of them aggregate in the B-cell follicle. Germinal centers are formed in the B-cell follicle with the tumor-derived antigen and tumor growth is accelerated.

Germinal centers are formed in the tumor-draining lymph node, indicating B-cell activation in response to tumors. To determine the role of B-cells in regulating tumor growth, I assessed E0771 breast cancer growth in several conditions. The tumor growth, germinal center formation, plasma IgG level and their co-relationship with B cell or CD169+ subcapsular sinus macrophages are summarized in **Table 4.1**. Briefly, tumor growth in B-cell deficient μMT mice plateaus at around day 13-15, while wild-type tumors continue grow until day 21 – the endpoint of my model. As expected, μMT tumor-draining lymph nodes show no germinal centers or the B-cell follicles. To further prove the necessity of B-cells in tumor growth, we transferred wild-type B-cells into μMT mice, which successfully recovered tumor growth, demonstrating the importance of B-cells in tumor growth. As germinal center formation occurs in the tumor-draining lymph node, I measured the production of IgG in tumor-bearing mice. Plasma IgG was increased in response to the tumor, suggesting B-cell activation. To determine the effect of B-cell activation on tumor growth, I attempted to accelerate tumor growth in wild-type mice with a plasma IgG transfer. As that yielded no significant results, I additionally attempted to recover tumor growth in μMT mice. This also failed to change tumor growth, suggesting the one-time plasma transfer as insufficient to promote tumor growth. Cumulatively, my project has conclusively deduced the necessity for B-cells, but not germinal center formation, in tumor growth. While minimal B-cells are enough to induce tumor growth, a one-time plasma IgG transfer is not. On the other hand, increased germinal center formation because of subcapsular sinus macrophage depletion is correlated with accelerated tumor growth, but no increase in plasma IgG levels.

Since $CD169^+$ subcapsular sinus macrophages suppressed B-cell activation, why do $CD169^+$ subcapsular sinus macrophages enter the germinal center in the tumor-draining lymph

node? There are a few potential explanations that can be described by comparing my results to published literature. Consistent with a melanoma mouse model, I found the $CD169^+$ subcapsular sinus macrophage layer became sparse in the tumor-draining lymph node [50]. My further studies determined that rather than depletion, these macrophages dissociated from the subcapsular sinus and some of them colocalized with germinal centers formed in tumor-draining lymph nodes. Their migration has previously been described to be CCR7-dependent during microbial infection induced inflammation in the draining lymph node [52]. As tumor-draining lymph nodes are also enlarged, it is possible that $CD169^+$ macrophage migration also depends on CCR7. This possibility can be tested using a CCR7 knockout model.

Subcapsular sinus macrophage function is closely related to the role of B-cells in murine tumor models. B-cells have been studied in the context of both melanoma and fibrosarcoma models. Both studies corroborate my account of a protumor B-cell activity subsequent to tumor implantation [49, 50]. In the melanoma model, tumor-derived vesicles are seen to penetrate deeper into the lymph node cortex, to the approximate depth of the B-cell follicles, like my observation of tumor-derived antigens found in the germinal center inside the B-cell follicles. These tumor-derived vesicles are retained at the subcapsular sinus by an intact $CD169^+$ macrophage layer in the tumor-draining lymph node [50]. Bypassing the subcapsular sinus macrophages by depleting the macrophages increased tumor-derived vesicles entering the B-cell zone, which is associated with increased plasma cell number and plasma IgG concentration. These results demonstrated that subcapsular sinus macrophages prevent B-cell activation.

In those studies, a one-time transfer of purified plasma IgG from the tumor-bearing mice to wild-type mice increased tumor growth as shown by the end tumor volume. These results did not complement my studies using a one-time plasma transfer before E0771 tumor implantation.

The one-time transfer of purified IgG suggests repetitive doses are not mandatory for tumor growth. Instead, there are other factors that may be responsible for my contrasting observations. First, it is possible that the transferred IgG from plasma is not sufficient to change tumor growth in my studies. Purified IgG, an increased amount of plasma transferred, or multiple plasma transfers might replicate the published observation in the melanoma model. Second, it is possible that melanoma tumor cells respond differently to tumor-induced immunoglobulins. Recently, a study using 4T1 breast cancer cells in BALB/c background mice have shown purified tumor-induced plasma IgG promotes metastasis but not tumor growth as opposed to the growth seen in melanoma [54]. Therefore, evidence already suggests different tumor types respond uniquely to immunoglobulins. Third, as my experiment consisted of transferring whole plasma into the animal instead of purifying IgG, it is possible the other plasma components (i.e. metabolites, enzymes, other proteins) may interfere with the interaction between immunoglobulins and tumor cells. Exploring these possibilities can better explain the function of tumor-induced IgG in the context of tumor growth.

It should be noted that IgG transfer only promoted tumor growth after being collected from subcapsular sinus macrophage-depleted CD169-DTR mice. These CD169-DTR mice show increased IgG production, but it is unclear if this was a consequence of diphtheria toxin treatment or increased tumor-derived vesicles in the tumor-draining lymph node cortex as an appropriate diphtheria toxin only-control was missing [50]. In my experiments using an E0771 tumor model, although I did observe more germinal centers in the tumor-draining lymph node, the overall level of plasma IgG was not significantly increased when subcapsular sinus macrophages are depleted with clodronate liposomes. Barring the previously described limitations with my experiments, it remains possible the plasma IgG isolated from the mice with a depleted subcapsular sinus

macrophage layer has different or higher affinity to tumor cells. I can test this idea by transferring IgG from PBS-liposome treated or clodronate liposome macrophage-depleted mice to determine if the observed tumor growth is diphtheria toxin specific, or if macrophage-depletion is sufficient. Further comparison of the plasma IgG isolated from different conditions might also give hints to the potential mechanism of how IgG regulates tumor growth.

In a recent study that aimed to elucidate the mechanism behind protumor B-cell activity, the authors also used a μMT mouse. Interestingly, using 4T1 breast cancer in BALB/c background μMT mice showed no difference in tumor size compared to wild-type, which is in contrast to my observations and the published melanoma model [54]. A potential explanation for this difference is that their μMT mouse model uses a BALB/c background, which have previously been shown to have imperfect B-cell deficiency, as μMT mice with a BALB/c background can produce high levels of all types of immunoglobulins [55, 56]. My studies were conducted in C57BL/6J background, which have also shown incomplete B-cell deficiency in μMT mice, but they only produce some IgG and IgE in an asthma model – ergo, more complete than the μMT BALB/c mouse model [57]. To exclude the possibility that there was residual IgG production in my model, I measured IgG level in μMT mice, and regardless of B-cell transfer, plasma IgG levels remained negligible. Therefore, it is likely the production of IgG is disease-specific, and E0771 breast cancer did not induce the production of IgG. Regardless, the difference in immunoglobulin production in μMT mice in different backgrounds may explain the contrasting observations seen in my studies and published literature.

While no consensus has been reached regarding the function of IgG, improved B-cell activity during tumor growth was highly consistent in animal models. There is also evidence of $tdTom^+$ B16F10 melanoma tumor-derived antigen deposition in the B-cell follicle, which is

associated with an increased IgG response, which complements my observations in the E0771-GFP tumor model [58]. While this observation is consistent with my data, depletion of subcapsular sinus macrophages inhibited tdTom^{+} B16F10 tumor-derived antigen deposition in the B-cell follicle, which creates another discrepancy between studies.

Cumulatively, my results confirm the essential nature of B-cell presence with respect to E0771 tumor growth. Due to all the controversies discussed, further studies are required to reveal the mechanism of how B-cells regulate tumor growth. While how germinal centers or antitumor IgG regulates tumor growth remains controversial, my studies indicate the B cells themselves might be more important than the IgG they produce. Tumor growth was suppressed in B-cell deficient μMT mice. This is consistent with other B-cell depletion models, as depleting B-cells with anti-CD20 also decelerated fibrosarcoma tumor growth [49]. However, even a minute proportion of B-cell recovery in μMT mice transferred with wild-type B cells was sufficient to restore tumor growth. From my results, it is clear that there was no restoration of plasma IgG or germinal center formation in those mice, thus the restored tumor growth was only dependent on B cells. My results indicate that IgG might not be important in regulating tumor growth using E0771 tumors. As such, a critical question remains: what is the function of the germinal centers?

As the role of germinal centers in the context of tumor progression remains to be elucidated, combining my results and evidence from the established literature, I generated a possible explanation for my observations. The activation of B-cells rather than germinal center immunoglobulins are required for baseline E0771 tumor growth, and germinal center IgG is used to accelerate it. This potentially explains why μMT tumor growth is recovered to wild-type levels upon B-cell transfer, despite the lack of germinal center formation. When wild-type mice have subcapsular sinus macrophages depleted, the number of germinal centers per lymph node

increased, alongside an increase in tumor growth. This demonstrates a correlation between germinal center formation and primary tumor growth acceleration.

The future direction of this project can first focus on the role of activated B-cells on tumor progression. I have clearly shown the importance of B-cells in tumor growth using a μMT B-cell deficient model. However, different B-cell depletion methods may have alternate effects on tumor progression. Different B-cell deficient mouse models can be used to determine if any method of B-cell depletion results in similar tumor progression and immunoglobulin production. Given that genetically modified B-cell deficient mouse models, such as the μMT mouse model, does not permit a specific timepoint of B-cell depletion, other B-cell depletion methods can be explored. Some of these B-cell depletion methods include the anti-CD20 antibody and CD19-DTR mice, which use controllable substances to manipulate B-cell presence. This will solidify the necessity of B-cells in tumor progression. Second, the role of germinal center formation in the tumor-draining lymph node can be further developed. As germinal center formation appears to be correlated with increased tumor growth, limiting germinal center formation in the tumor-draining lymph node can imply their role in tumor progression. Administering interleukin-2 has been shown to inhibit germinal center formation in influenza models, thus a similar model can be applied to tumors [59]. This can also help identify any differences in immunoglobulin production by the germinal centers by identifying changes in immunoglobulin levels between control and B-cell deficient groups. Third, the function of subcapsular sinus macrophages within the germinal centers can be elucidated. These macrophages can potentially play a role in changing the type or the function of the immunoglobulins produced by the germinal center. Fourth, the project can focus on the immunoglobulins in tumor-bearing mice and their functions. Quantifying different immunoglobulin types in tumor-bearing mice can reveal a previously undiscovered player in

E0771 tumor growth. This may explain the discrepancy in observations in μMT mice tumor growth given their differences in immunoglobulin production. These immunoglobulins can be studied for their affinity to tumor cells, and the consequences for their binding. This can help describe the mechanism by which immunoglobulins affect tumor progression. Finally, a culmination of these results can contribute to the overall goal of this project; identifying new targets for cancer immunotherapy. As it has been previously shown that B-cells affect the production of regulatory T-cells, $CD8^+$ T-cells, and $CD4^+$ T-cells, understanding the interplay between the tumor-activated immunoglobulins and these T-cells can have significant implications on cancer immunotherapy [49]. Understanding both the mechanism and the players involved in pro-tumor B-cells can lead to the development of combinational therapies that can be used for patients that are currently untreatable with today's methods.

In conclusion, this project reveals the importance of B-cells in the context of tumor progression. While the limitation of immunotherapies surrounding antitumor T-cells is getting clearer, other aspects of tumor immunity are required to reveal the mechanisms or develop alternative solutions. My studies revealed the necessity of B-cells for tumor growth. Additionally, I demonstrated lymph node B-cell activation in response to tumors and revealed the role of subcapsular sinus macrophages in limiting this activation. While I did not completely exclude IgG from the possible factors that induce tumor progression, I have demonstrated that in the E0771 breast cancer model, a single plasma IgG transfer is not enough to restore tumor growth in wild type or B-cell deficient mice. I have also demonstrated no change in IgG production, despite an increase in lymph node B-cell activation. This leaves several directions open for future experiments, such as the function of germinal centers in the lymph nodes, and the B-cell mechanism to increase tumor progression. Completing these future directions can improve

the development of cancer immunotherapies and provide options for patients that are not responsive to the well-developed T-cell cancer immunotherapies.

Table 4.1: Summary of observations in experimental mouse models

Mouse Model	**Phenotype**				
	Tumor Growth	*B-cells*	*Germinal Center Formation*	*Subcapsular sinus macrophages*	*Plasma IgG*
Control	*N/A*	++	-	++	+
Wild-Type	++	++	++	++	++
µMT	+	-	-	-	-
µMT with wild-type B-cells	++	+	-	++	-
µMT with wild-type plasma	+	-	-	-	-
PBS liposome	++	++	++	++	++
Clodronate liposome	+++	++	+++	-	++

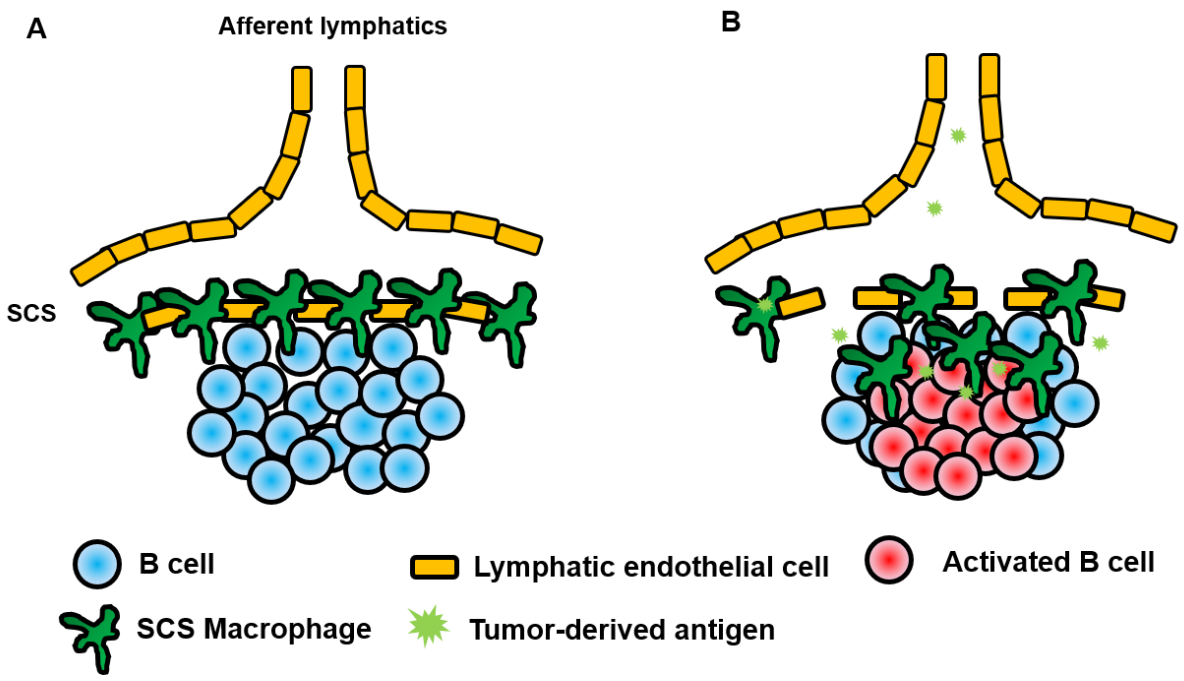

Figure 4.1: Schematic figure of B-cell activation in an E0771 tumor-draining lymph node. A normal lymph node consists of a layer of macrophages underlying the subcapsular sinus that prevent the entry of lymph-borne pathogens. Underneath these macrophages are the B-cell follicles, which can interact with the subcapsular sinus macrophages for immune activation (**A**). In tumor-draining lymph nodes, the subcapsular sinus macrophage layer is disrupted, and many of the macrophages migrate into the B-cell follicle. This allows tumor-derived antigens to penetrate into the lymph node cortex and aggregate in the B-cell follicle. B-cell activation occurs in the form of a germinal center, and the tumor-derived antigens accumulate with the activated B-cells, potentially inducing the production of pro-tumor immunoglobulins (**B**).

LITERATURE CITED:

1. Seyfried TN, Huysentruyt LC: **On the origin of cancer metastasis.** *Crit Rev Oncog* 2013, **18:**43-73.
2. Khanfir A, Lahiani F, Bouzguenda R, Ayedi I, Daoud J, Frikha M: **Prognostic factors and survival in metastatic breast cancer: A single institution experience.** *Rep Pract Oncol Radiother* 2013, **18:**127-132.
3. Asano T, Ohnishi K, Shiota T, Motoshima T, Sugiyama Y, Yatsuda J, Kamba T, Ishizaka K, Komohara Y: **CD169-positive sinus macrophages in the lymph nodes determine bladder cancer prognosis.** *Cancer Sci* 2018, **109:**1723-1730.
4. Schoppmann SF, Birner P, Stöckl J, Kalt R, Ullrich R, Caucig C, Kriehuber E, Nagy K, Alitalo K, Kerjaschki D: **Tumor-associated macrophages express lymphatic endothelial growth factors and are related to peritumoral lymphangiogenesis.** *Am J Pathol* 2002, **161:**947-956.
5. Akagi K, Ikeda Y, Miyazaki M, Abe T, Kinoshita J, Maehara Y, Sugimachi K: **Vascular endothelial growth factor-C (VEGF-C) expression in human colorectal cancer tissues.** *Br J Cancer* 2000, **83:**887-891.
6. George ML, Tutton MG, Janssen F, Arnaout A, Abulafi AM, Eccles SA, Swift RI: **VEGF-A, VEGF-C, and VEGF-D in colorectal cancer progression.** *Neoplasia* 2001, **3:**420-427.
7. Salven P, Lymboussaki A, Heikkilä P, Jääskela-Saari H, Enholm B, Aase K, von Euler G, Eriksson U, Alitalo K, Joensuu H: **Vascular endothelial growth factors VEGF-B and VEGF-C are expressed in human tumors.** *Am J Pathol* 1998, **153:**103-108.
8. Skobe M, Hawighorst T, Jackson DG, Prevo R, Janes L, Velasco P, Riccardi L, Alitalo K, Claffey K, Detmar M: **Induction of tumor lymphangiogenesis by VEGF-C promotes breast cancer metastasis.** *Nat Med* 2001, **7:**192-198.
9. Förster R, Schubel A, Breitfeld D, Kremmer E, Renner-Müller I, Wolf E, Lipp M: **CCR7 coordinates the primary immune response by establishing functional microenvironments in secondary lymphoid organs.** *Cell* 1999, **99:**23-33.
10. Saeki H, Moore AM, Brown MJ, Hwang ST: **Cutting edge: secondary lymphoid-tissue chemokine (SLC) and CC chemokine receptor 7 (CCR7) participate in the emigration pathway of mature dendritic cells from the skin to regional lymph nodes.** *J Immunol* 1999, **162:**2472-2475.
11. Cabioglu N, Yazici MS, Arun B, Broglio KR, Hortobagyi GN, Price JE, Sahin A: **CCR7 and CXCR4 as novel biomarkers predicting axillary lymph node metastasis in T1 breast cancer.** *Clin Cancer Res* 2005, **11:**5686-5693.
12. Randolph GJ, Ivanov S, Zinselmeyer BH, Scallan JP: **The Lymphatic System: Integral Roles in Immunity.** *Annu Rev Immunol* 2017, **35:**31-52.
13. Drayton DL, Liao S, Mounzer RH, Ruddle NH: **Lymphoid organ development: from ontogeny to neogenesis.** *Nat Immunol* 2006, **7:**344-353.
14. Liao S, von der Weid PY: **Lymphatic system: an active pathway for immune protection.** *Semin Cell Dev Biol* 2015, **38:**83-89.
15. Ohl L, Mohaupt M, Czeloth N, Hintzen G, Kiafard Z, Zwirner J, Blankenstein T, Henning G, Förster R: **CCR7 governs skin dendritic cell migration under inflammatory and steady-state conditions.** *Immunity* 2004, **21:**279-288.

16. Pflicke H, Sixt M: **Preformed portals facilitate dendritic cell entry into afferent lymphatic vessels.** *J Exp Med* 2009, **206:**2925-2935.
17. Nitschke M, Aebischer D, Abadier M, Haener S, Lucic M, Vigl B, Luche H, Fehling HJ, Biehlmaier O, Lyck R, Halin C: **Differential requirement for ROCK in dendritic cell migration within lymphatic capillaries in steady-state and inflammation.** *Blood* 2012, **120:**2249-2258.
18. Beauvillain C, Cunin P, Doni A, Scotet M, Jaillon S, Loiry ML, Magistrelli G, Masternak K, Chevailler A, Delneste Y, Jeannin P: **CCR7 is involved in the migration of neutrophils to lymph nodes.** *Blood* 2011, **117:**1196-1204.
19. Cao C, Lawrence DA, Strickland DK, Zhang L: **A specific role of integrin Mac-1 in accelerated macrophage efflux to the lymphatics.** *Blood* 2005, **106:**3234-3241.
20. Gray EE, Cyster JG: **Lymph node macrophages.** *J Innate Immun* 2012, **4:**424-436.
21. Kuka M, Iannacone M: **The role of lymph node sinus macrophages in host defense.** *Ann N Y Acad Sci* 2014, **1319:**38-46.
22. Phan TG, Green JA, Gray EE, Xu Y, Cyster JG: **Immune complex relay by subcapsular sinus macrophages and noncognate B cells drives antibody affinity maturation.** *Nat Immunol* 2009, **10:**786-793.
23. Asano K, Nabeyama A, Miyake Y, Qiu CH, Kurita A, Tomura M, Kanagawa O, Fujii S, Tanaka M: **CD169-positive macrophages dominate antitumor immunity by crosspresenting dead cell-associated antigens.** *Immunity* 2011, **34:**85-95.
24. Gerner MY, Torabi-Parizi P, Germain RN: **Strategically localized dendritic cells promote rapid T cell responses to lymph-borne particulate antigens.** *Immunity* 2015, **42:**172-185.
25. Witmer-Pack MD, Hughes DA, Schuler G, Lawson L, McWilliam A, Inaba K, Steinman RM, Gordon S: **Identification of macrophages and dendritic cells in the osteopetrotic (op/op) mouse.** *J Cell Sci* 1993, **104 (Pt 4):**1021-1029.
26. MacDonald KP, Palmer JS, Cronau S, Seppanen E, Olver S, Raffelt NC, Kuns R, Pettit AR, Clouston A, Wainwright B, et al: **An antibody against the colony-stimulating factor 1 receptor depletes the resident subset of monocytes and tissue- and tumor-associated macrophages but does not inhibit inflammation.** *Blood* 2010, **116:**3955-3963.
27. Chávez-Galán L, Olleros ML, Vesin D, Garcia I: **Much More than M1 and M2 Macrophages, There are also CD169(+) and TCR(+) Macrophages.** *Front Immunol* 2015, **6:**263.
28. Steer HW, Foot RA: **Changes in the medulla of the parathymic lymph nodes of the rat during acute gastro-intestinal inflammation.** *J Anat* 1987, **152:**23-36.
29. Nossal GJ, Abbot A, Mitchell J: **Antigens in immunity. XIV. Electron microscopic radioautographic studies of antigen capture in the lymph node medulla.** *J Exp Med* 1968, **127:**263-276.
30. Iannacone M, Moseman EA, Tonti E, Bosurgi L, Junt T, Henrickson SE, Whelan SP, Guidotti LG, von Andrian UH: **Subcapsular sinus macrophages prevent CNS invasion on peripheral infection with a neurotropic virus.** *Nature* 2010, **465:**1079-1083.
31. Moseman EA, Iannacone M, Bosurgi L, Tonti E, Chevrier N, Tumanov A, Fu YX, Hacohen N, von Andrian UH: **B cell maintenance of subcapsular sinus macrophages protects against a fatal viral infection independent of adaptive immunity.** *Immunity* 2012, **36:**415-426.

32. Junt T, Moseman EA, Iannacone M, Massberg S, Lang PA, Boes M, Fink K, Henrickson SE, Shayakhmetov DM, Di Paolo NC, et al: **Subcapsular sinus macrophages in lymph nodes clear lymph-borne viruses and present them to antiviral B cells.** *Nature* 2007, **450:**110-114.
33. Farrell HE, Davis-Poynter N, Bruce K, Lawler C, Dolken L, Mach M, Stevenson PG: **Lymph Node Macrophages Restrict Murine Cytomegalovirus Dissemination.** *J Virol* 2015, **89:**7147-7158.
34. Kastenmüller W, Torabi-Parizi P, Subramanian N, Lämmermann T, Germain RN: **A spatially-organized multicellular innate immune response in lymph nodes limits systemic pathogen spread.** *Cell* 2012, **150:**1235-1248.
35. Barral P, Polzella P, Bruckbauer A, van Rooijen N, Besra GS, Cerundolo V, Batista FD: **CD169(+) macrophages present lipid antigens to mediate early activation of iNKT cells in lymph nodes.** *Nat Immunol* 2010, **11:**303-312.
36. Saunderson SC, Dunn AC, Crocker PR, McLellan AD: **CD169 mediates the capture of exosomes in spleen and lymph node.** *Blood* 2014, **123:**208-216.
37. Ohnishi K, Komohara Y, Saito Y, Miyamoto Y, Watanabe M, Baba H, Takeya M: **CD169-positive macrophages in regional lymph nodes are associated with a favorable prognosis in patients with colorectal carcinoma.** *Cancer Sci* 2013, **104:**1237-1244.
38. Shiota T, Miyasato Y, Ohnishi K, Yamamoto-Ibusuki M, Yamamoto Y, Iwase H, Takeya M, Komohara Y: **The Clinical Significance of CD169-Positive Lymph Node Macrophage in Patients with Breast Cancer.** *PLoS One* 2016, **11:**e0166680.
39. Erdag G, Schaefer JT, Smolkin ME, Deacon DH, Shea SM, Dengel LT, Patterson JW, Slingluff CL: **Immunotype and immunohistologic characteristics of tumor-infiltrating immune cells are associated with clinical outcome in metastatic melanoma.** *Cancer Res* 2012, **72:**1070-1080.
40. Hiraoka K, Miyamoto M, Cho Y, Suzuoki M, Oshikiri T, Nakakubo Y, Itoh T, Ohbuchi T, Kondo S, Katoh H: **Concurrent infiltration by CD8+ T cells and CD4+ T cells is a favourable prognostic factor in non-small-cell lung carcinoma.** *Br J Cancer* 2006, **94:**275-280.
41. Hung K, Hayashi R, Lafond-Walker A, Lowenstein C, Pardoll D, Levitsky H: **The central role of CD4(+) T cells in the antitumor immune response.** *J Exp Med* 1998, **188:**2357-2368.
42. Nguyen HH, Kim T, Song SY, Park S, Cho HH, Jung SH, Ahn JS, Kim HJ, Lee JJ, Kim HO, et al: **Naïve CD8(+) T cell derived tumor-specific cytotoxic effectors as a potential remedy for overcoming TGF-β immunosuppression in the tumor microenvironment.** *Sci Rep* 2016, **6:**28208.
43. Yu J, Tian R, Xiu B, Yan J, Jia R, Zhang L, Chang AE, Song H, Li Q: **Antitumor activity of T cells generated from lymph nodes draining the SEA-expressing murine B16 melanoma and secondarily activated with dendritic cells.** *Int J Biol Sci* 2009, **5:**135-146.
44. Porter DL, Levine BL, Kalos M, Bagg A, June CH: **Chimeric antigen receptor-modified T cells in chronic lymphoid leukemia.** *N Engl J Med* 2011, **365:**725-733.
45. Richards RM, Sotillo E, Majzner RG: **CAR T Cell Therapy for Neuroblastoma.** *Front Immunol* 2018, **9:**2380.

46. Buchbinder EI, Desai A: **CTLA-4 and PD-1 Pathways: Similarities, Differences, and Implications of Their Inhibition.** *Am J Clin Oncol* 2016, **39:**98-106.
47. Hodi FS, O'Day SJ, McDermott DF, Weber RW, Sosman JA, Haanen JB, Gonzalez R, Robert C, Schadendorf D, Hassel JC, et al: **Improved survival with ipilimumab in patients with metastatic melanoma.** *N Engl J Med* 2010, **363:**711-723.
48. Topalian SL, Hodi FS, Brahmer JR, Gettinger SN, Smith DC, McDermott DF, Powderly JD, Carvajal RD, Sosman JA, Atkins MB, et al: **Safety, activity, and immune correlates of anti-PD-1 antibody in cancer.** *N Engl J Med* 2012, **366:**2443-2454.
49. Maglioco A, Machuca DG, Badano MN, Nannini P, Camerano GV, Costa H, Meiss R, Ruggiero RA, Giordano M, Dran GI: **B cells inhibit the antitumor immunity against an established murine fibrosarcoma.** *Oncol Lett* 2017, **13:**3225-3232.
50. Pucci F, Garris C, Lai CP, Newton A, Pfirschke C, Engblom C, Alvarez D, Sprachman M, Evavold C, Magnuson A, et al: **SCS macrophages suppress melanoma by restricting tumor-derived vesicle-B cell interactions.** *Science* 2016, **352:**242-246.
51. Ewens A, Mihich E, Ehrke MJ: **Distant metastasis from subcutaneously grown E0771 medullary breast adenocarcinoma.** *Anticancer Res* 2005, **25:**3905-3915.
52. Gaya M, Castello A, Montaner B, Rogers N, Reis e Sousa C, Bruckbauer A, Batista FD: **Host response. Inflammation-induced disruption of SCS macrophages impairs B cell responses to secondary infection.** *Science* 2015, **347:**667-672.
53. Kitamura D, Roes J, Kühn R, Rajewsky K: **A B cell-deficient mouse by targeted disruption of the membrane exon of the immunoglobulin mu chain gene.** *Nature* 1991, **350:**423-426.
54. Gu Y, Liu Y, Fu L, Zhai L, Zhu J, Han Y, Jiang Y, Zhang Y, Zhang P, Jiang Z, Zhang X, Cao X: **Tumor-educated B cells selectively promote breast cancer lymph node metastasis by HSPA4-targeting IgG.** *Nature Medicine* 2019, **25:**312-322.
55. Hasan M, Polic B, Bralic M, Jonjic S, Rajewsky K: **Incomplete block of B cell development and immunoglobulin production in mice carrying the muMT mutation on the BALB/c background.** *European Journal of Immunology* 2002, **32:**3463-3471.
56. Orinska Z, Osiak A, Löhler J, Bulanova E, Budagian V, Horak I, Bulfone-Paus S: **Novel B cell population producing functional IgG in the absence of membrane IgM expression.** *Eur J Immunol* 2002, **32:**3472-3480.
57. Ghosh S, Hoselton SA, Schuh JM: **μ-chain-deficient mice possess B-1 cells and produce IgG and IgE, but not IgA, following systemic sensitization and inhalational challenge in a fungal asthma model.** *J Immunol* 2012, **189:**1322-1329.
58. Moalli F, Proulx ST, Schwendener R, Detmar M, Schlapbach C, Stein JV: **Intravital and whole-organ imaging reveals capture of melanoma-derived antigen by lymph node subcapsular macrophages leading to widespread deposition on follicular dendritic cells.** *Front Immunol* 2015, **6:**114.
59. Ballesteros-Tato A, León B, Graf BA, Moquin A, Adams PS, Lund FE, Randall TD: **Interleukin-2 inhibits germinal center formation by limiting T follicular helper cell differentiation.** *Immunity* 2012, **36:**847-856.

APPENDIX:

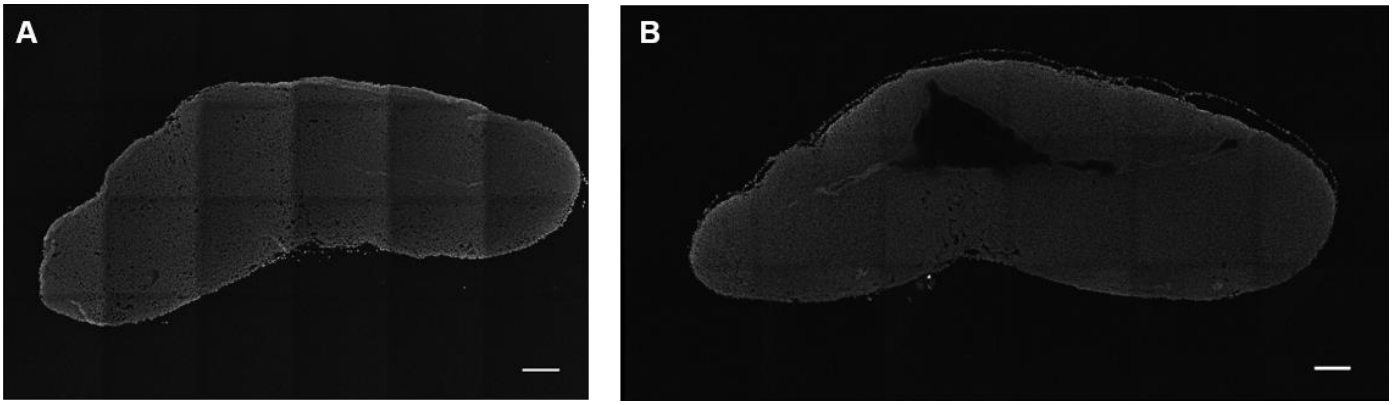

Supplemental Figure 1: Negative controls for E0771 non-draining lymph node and tumor-draining lymph node. A, B. Immunofluorescent images of E0771 non-draining lymph node and tumor-draining lymph node with only secondary antibodies and DAPI to confirm lymph node location (scale bar: 200μm, original magnification: 200x). DAPI (white), Alexa Fluor 488 (green), Cy3 (red), Cy5 (blue). Representative images of n = 3.

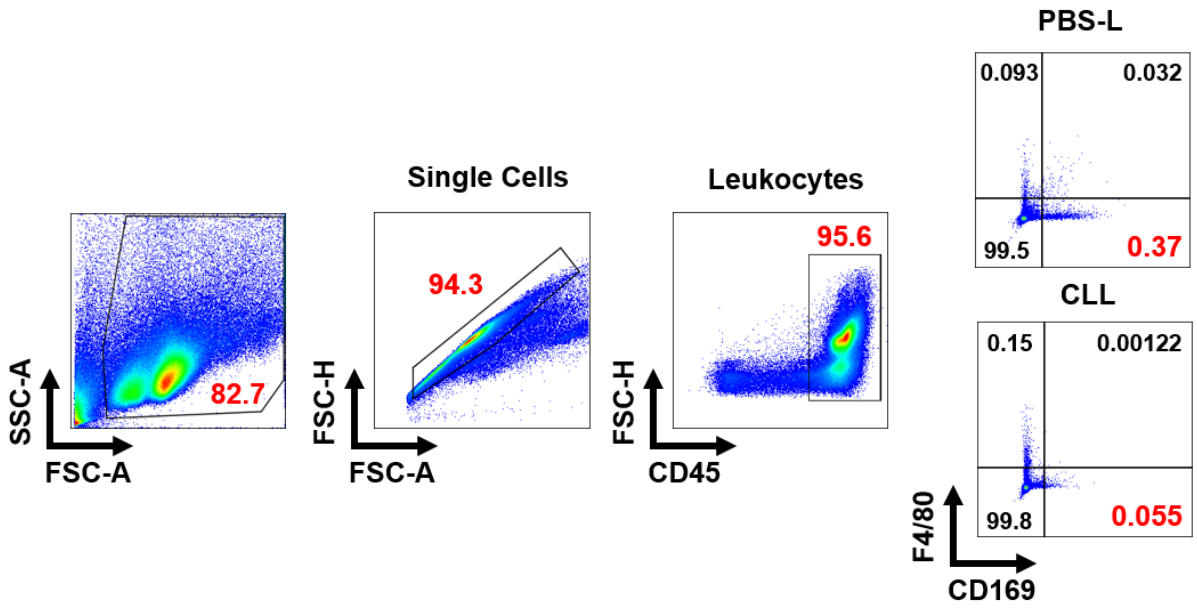

Supplemental Figure 2: Sample lymph node flow cytometry gating strategy. Flow cytometry gating strategy for lymph nodes to study cell populations. Cell debris is excluded using a forward scatter and side scatter plot. Then single cells are selected using a forward scatter area by forward scatter height plot. Immune cells are selected using the common leukocyte antigen marker CD45. Specific immune cell populations are plotted and analyzed using various markers.

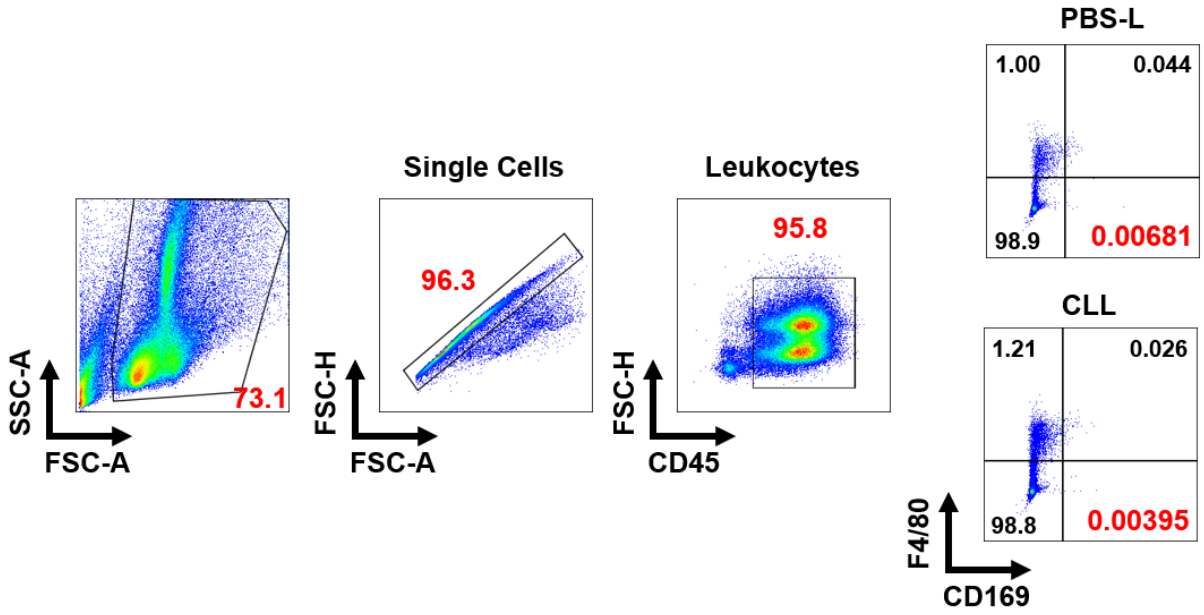

Supplemental Figure 3: Sample spleen flow cytometry gating strategy. Flow cytometry gating strategy for spleens to study cell populations. Cell debris is excluded using a forward scatter and side scatter plot. Then single cells are selected using a forward scatter area by forward scatter height plot. Immune cells are selected using the common leukocyte antigen marker CD45. Specific immune cell populations are plotted and analyzed using various markers.

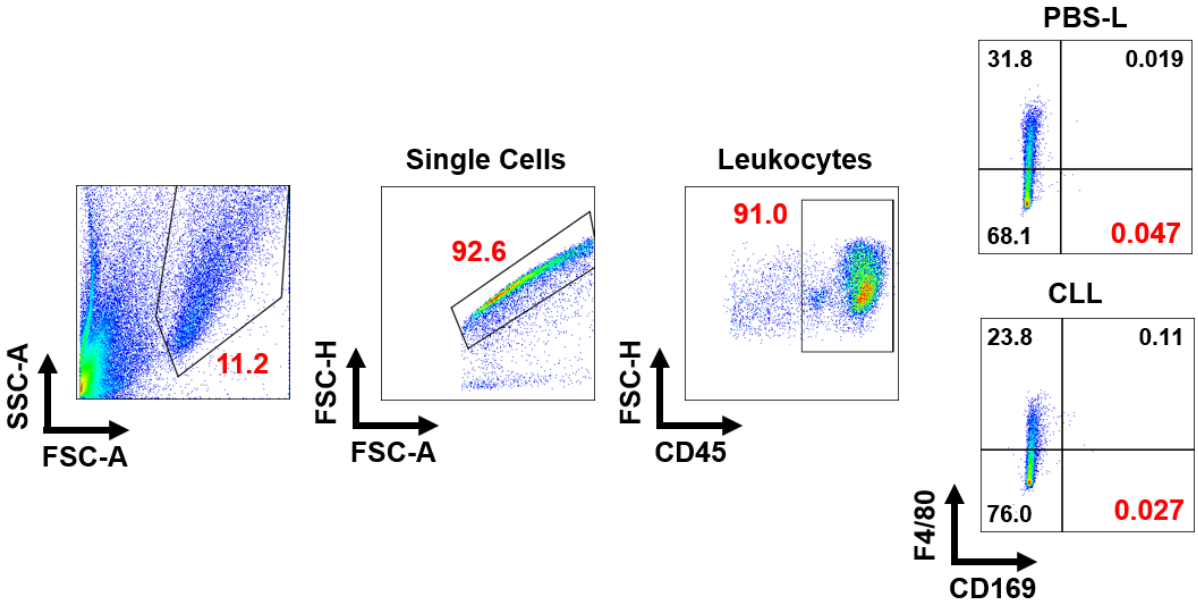

Supplemental Figure 4: Sample tumor flow cytometry gating strategy. Flow cytometry gating strategy for tumors to study cell populations. Cell debris is excluded using a forward scatter and side scatter plot. Then single cells are selected using a forward scatter area by forward scatter height plot. Immune cells are selected using the common leukocyte antigen marker CD45. Specific immune cell populations are plotted and analyzed using various markers.